

AD-A250 306



**UNIVERSITY OF SOUTHERN CALIFORNIA
SCHOOL OF ENGINEERING**

2

UNIVERSITY RESEARCH INITIATIVE

**CENTER FOR THE INTEGRATION
OF
OPTICAL COMPUTING**

AFOSR-90-0133

AEOSR-IR- 92 0279

SECOND ANNUAL TECHNICAL REPORT

FOR THE PERIOD

February 15, 1991 through February 14, 1992

Presented To:

DISTRIBUTION STATEMENT A

**Approved for public release
Distribution Unlimited**

Air Force Office of Scientific Research

Building 410

Attn.: XOT (Room A115)

Bolling AFB, DC 20332-6448

Presented By:

University of Southern California

School of Engineering

Los Angeles, California 90089-0483

Principal Investigators

A.A. Sawchuk and W. H. Steier

**DTIC
SELECTE
MAY 18 1992
S B D**

REPORT DOCUMENTATION PAGE

OMB No. 0704-0188

Public reporting burden for this collection of information is estimated to average 1 hour per response, including the time for reviewing instructions, searching existing data sources, gathering and maintaining the data needed, and completing and reviewing the collection of information. Send comments regarding this burden estimate or any other aspect of this collection of information, including suggestions for reducing this burden, to Washington Headquarters Service, Directorate for Information Operations and Reports, 1215 Jefferson Davis Highway, Suite 1204, Arlington, VA 22202-4302, and to the Office of Management and Budget, Paperwork Reduction Project (0704-0188), Washington, DC 20503.

1. AGENCY USE ONLY (Leave blank)	2. REPORT DATE 3/15/92	3. REPORT TYPE AND DATES COVERED 2nd annual tech report 2/15/91-2/14/92
----------------------------------	---------------------------	---

4. TITLE AND SUBTITLE CENTER FOR THE INTEGRATION OF OPTICAL COMPUTING	5. FUNDING NUMBERS AFOSR -90-0133
--	--------------------------------------

6. AUTHOR(S) PRINCIPAL INVESTIGATORS: A.A. SAWCHUK - W.H. STEIER
--

7. PERFORMING ORGANIZATION NAME(S) AND ADDRESS(ES) UNIVERSITY OF SOUTHERN CALIFORNIA DEPT. OF ELECTRICAL ENGINEERING / ELECTROPHYSICS SEAVER SCIENCE CENTER 502 LOS ANGELES, CA 90087/0483	8. PERFORMING ORGANIZATION REPORT NUMBER
--	--

9. SPONSORING / MONITORING AGENCY NAME(S) AND ADDRESS(ES) AIR FORCE OFFICE OF SCIENTIFIC RESEARCH BUILDING 410 BOLLING AIR FORCE BASE D.C. 20332-6448 <i>Craig</i>	10. SPONSORING / MONITORING AGENCY REPORT NUMBER <i>NE</i> <i>3484 AB</i>
---	---

11. SUPPLEMENTARY NOTES

12a. DISTRIBUTION / AVAILABILITY STATEMENT <i>unlimited</i>	12b. DISTRIBUTION CODE
--	------------------------

13. ABSTRACT (Maximum 200 words) Topics reviewed include: Optical connections, lenslet array processors, generalization neural networks, spatial light modulators, MBE growth of quantum well structures, ultralow threshold laser array, charge transport optical nonlinearities, wave mixing at the bandedge in III-V semiconductors and photorefractive optical interconnections
--

14. SUBJECT TERMS Optical computing, laser arrays, spatial modulators, optical interconnections, optical neural interconnections.	15. NUMBER OF PAGES 53
	16. PRICE CODE

17. SECURITY CLASSIFICATION OF REPORT <i>unclass</i>	18. SECURITY CLASSIFICATION OF THIS PAGE <i>unclass</i>	19. SECURITY CLASSIFICATION OF ABSTRACT <i>unclass</i>	20. LIMITATION OF ABSTRACT <i>UL</i>
---	--	---	---

UNIVERSITY RESEARCH INITIATIVE

**CENTER FOR THE INTEGRATION
OF
OPTICAL COMPUTING**

AFOSR-90-0133

SECOND ANNUAL TECHNICAL REPORT

FOR THE PERIOD

February 15, 1991 through February 14, 1992

Presented To:

**Air Force Office of Scientific Research
Building 410
Attn.: XOT (Room A115)
Bolling AFB, DC 20332-6448**

Presented By:

**University of Southern California
School of Engineering
Los Angeles, California 90089-0483**

Principal Investigators

A.A. Sawchuk and W. H. Steier

TABLE OF CONTENTS

I.	DIRECTOR'S OVERVIEW	
II.	THE RESEARCH	
	Dynamic Optical Interconnection Networks with Integrated Optoelectronic Transceivers A.A. Sawchuk and S.R. Forrest	1
	Interconnections and Spatial Light Modulators for Generalizable Photonic Neural Networks A. R. Tanguay, Jr.	10
	MBE Growth of Quantum Well Structures for Generalizable Photonic Neural Networks A. Madhukar	18
	Cloning Of Generalizable Photonic Neural Network Interconnections B. K. Jenkins	23
	Ultralow Threshold Laser Arrays - P.D. Dapkus	30
	Optical Interconnections and Optical Neurons Using Charge Transport Optical Nonlinearities W.H. Steier	36
	Optical Interconnections Using Wave Mixing at the Bandedge in III-V Semiconductor Depletion Regions E. Garmire	42
	Photorefractive Optical Interconnections J. Feinberg	44
III.	Publications and Presentations	49

DIRECTORS OVERVIEW

This technical report summarizes the progress made under the University Research Initiative Center for the Integration of Optical Computing, Contract AFOSR 90-0133 for the period 2/15/91 through 2/14/92. This is the second year of the second three year period of research.

From the outset the goals of the Center for the Integration of Optical Computing have been: 1) to perform research which is at the forefront of optical computing in the areas of materials, devices, and architectures, 2) to conceive and direct the research in selected demonstration projects which combine the efforts of several faculty, and 3) to develop common laboratory space and facilities which bring together the students and faculty from the often diverse areas of devices, materials, and architectures to stimulate interactions. In all of these goals we have made great progress while the Center has been in existence and have continued that progress in the past year.

The first demonstration project "Dynamic Optical Interconnection Networks with Integrated Optoelectronic Transceivers" is reported on in some detail by Professors S. R. Forrest and A. A. Sawchuk. This project has now been expanded to include a more efficient photopolymer holographic material. The low efficiency of the earlier silver halide materials was a previous bottleneck. This project combines the materials, devices, and systems expertise of the faculty toward the realization of a high density and high bandwidth optoelectronic interconnection network.

The second demonstration project "Generalizable Photonic Neural Networks" is reported on by Professors A. R. Tanguay, Jr., B. K. Jenkins, and A. Madhukar. The goals of this work are to develop the materials capability, the device structures, and the architecture for realizing a generalizable and highly parallel neural network which is manufacturable. This project is reported on in three separate sections of the reports. Significant progress has been made in the MQW modulators and switches, in architecture analysis, and in the cloning of master holographic interconnections

In addition we are reporting on four research projects which are directed toward the building of the technology base for optical computing. These four projects are focused on various bottlenecks in materials, devices, and systems which stand in the way of the

realization of a practical optical computer. This includes work on arrays of low threshold lasers by Prof. P. D. Dapkus, optical interconnections using the optical nonlinearities at the band edge of semiconductors by Prof. E. Garmire, a study of photorefractive interconnects using mutually pumped phase conjugators by Prof. J. Feinberg, and a study of methods to improve the sensitivity and magnitude of infrared photorefractive in semiconductors for use in optical neurons and switches by Prof. W. H. Steier.

The report closes with a listing of the publications and presentations of the faculty during the past year concerning the research on optical computing. As evidenced by the 37 publications and presentations listed and the three patents applied for, this has been a productive year for the program.

Accession For	
NTIS GRA&I	<input checked="" type="checkbox"/>
DTIC TAB	<input type="checkbox"/>
Unannounced	<input type="checkbox"/>
Justification	
By _____	
Distribution/	
Availability Codes	
Dist	Avail and/or Special
A-1	



Dynamic Optical Interconnection Networks with Integrated Optoelectronic Transceivers

A. A. Sawchuk and S. R. Forrest

Earlier in this program, we have developed several multistage architectures for dynamic optical interconnection networks [1]. In these architectures, the interconnection between any input and any output is achieved by cascaded stages of fixed optical interconnections interleaved with dynamic switches as the fixed interconnections at every stage. Optoelectronic switch arrays are used for the dynamic switching in between the stages of 2-D perfect shuffles. One concept for the implementation of high density, high bandwidth dynamic local interconnections has been demonstrated with optically powered 2x2 optoelectronic switches using polarization control [2]. These switches had crosstalk less than -50 dB. We have also developed a light efficient algorithm to perform 2-D perfect shuffles optically, and have demonstrated the principle of using silver halide holograms [3]-[5]. However, the desired high efficiency can not be achieved due to the low diffraction efficiency of the silver halide material (measured at only 2.9%). This creates problems for a passive network when the regeneration of signals is not possible at every stage.

During the past year, we have worked on implementing the optical 2-D perfect shuffles using DuPont holographic transmission photopolymer material. We have achieved more than 60% effective light efficiency after considering the absorption and the reflection of the material. In this experiment, the same light efficient algorithm illustrated in Fig. 1 is used. The input plane is first magnified twice. A four facet hologram is used as a holographic prism array to perform different deflection operations on the four quadrants of the magnified input. The four quadrants are deflected and superimposed on the output plane as a 2-D perfect shuffled result.

Figure 2 shows the experimental setup. The two beams shown shaded are used to make the facet hologram on the hologram plane. A specially designed mask at the hologram plane allows only one quadrant to be exposed at a time. We adjust lens L_4 in both horizontal and vertical directions for each exposure to get different deflection angles for each facet. In reconstruction, the reference beam is blocked, and the pre-magnified input plane is inserted. The 4-f optical system projects the four quadrants on the corresponding facets of the hologram. The superposition of these four deflected quadrants appears at the observation plane and shows the shuffled result. The pre-magnified input plane is an 8x8 binary

inverse perfect shuffled letter *H*. It is generated by computer and photoreduced to get a 10 mm x 10 mm pattern. Thus, each pixel has diameter 0.31 mm and the center-to-center distance between two neighboring pixels is 1.25 mm.

From our measurements, we found the optimum exposure energy for DuPont photopolymer is approximately 100 mJ/cm². The photopolymer hologram needs a UV curing process, which polymerizes the monomers not exposed to light. The fixing energy is around 577 mJ/cm². The changes in the exposure energy and the fixing energy influence the final diffraction efficiency of a hologram. In our experiment, the optimum exposure energy for each facet is applied. After the recording, the photopolymer hologram is cured by a UV light source but the fixing energy is not optimized. Figure 3 shows the simulated and experimental results. The real diffraction efficiency, which is defined as the ratio of the intensity of the diffracted light to the incident light, is found to be 60% averaged over the four facets. The scattering of the photopolymer is around 21% and the reflection loss is about 9.2%. However, the effective diffraction efficiency, which is defined to be the ratio of the diffracted light to the sum of the diffracted and the zeroth order light, is measured to be 93.8% on average.

This result demonstrated that high light efficiency optical 2-D perfect shuffles can be achieved when a high optical efficiency algorithm is used in combination with proper optical components. Parameters such as the exposure and fixing energies for hologram preparation must be optimized to get high efficiency.

The work on interconnection architectures has been accompanied by significant progress in the area of optoelectronic optical logic circuits using optical powering. As noted in past reports, the performance of high density, high bandwidth 2D and 3D optoelectronic interconnections used in optical processing, computing and communications systems is ultimately limited by crosstalk between neighboring functional elements (or pixels) on the arrays which commonly comprise such interconnection architectures. Crosstalk can have numerous sources, including thermal, optical and electrical. In general, the high frequency performance limit of many optoelectronic 2D pixel arrays is set by electrical crosstalk to lie in the 200 MHz–500 MHz range. In work being pursued in our laboratory, therefore, we have concentrated on investigating architectures which are *not* intrinsically limited by crosstalk induced by capacitive and inductive coupling between neighboring pixels. Our approach has been to consider

the use of optical sources as a means to apply power independently to each pixel in a large-scale, 2D array. In practice, this is accomplished by integrating a photovoltaic cell array along with each optoelectronic pixel, and then illuminating the cell with a high power GaAs laser diode. Supplying local power in this manner has the advantage of providing an inductance and capacitance-free power source.(i.e., photons), and it eliminates space-consuming power supply lines and capacitive decoupling circuitry at each pixel. In a recent analysis of such a system [6], it was found that optically powered 2D optoelectronic switching arrays can be operated at frequencies at least one order of magnitude higher than similar arrays which are electrically powered.

A possible architecture for an optically powered 3D optoelectronic interconnect is illustrated in Fig. 4. Here, to eliminate optical crosstalk between the power and data beams, the two signals are introduced at different wavelengths. For the purposes of illustration, the data is transmitted between interconnection layers at 1.3 μm wavelength, whereas power is supplied by an 0.8 μm wavelength GaAs laser. In the figure, each pixel is shown to have an optical detector (possibly $\text{In}_{0.53}\text{Ga}_{0.47}\text{As}$ lattice-matched to an InP substrate) sensitive to the long wavelength light for data input, some data processing electronics, and a low threshold laser diode as the output device. Of course, the detector/laser approach can be replaced by optical modulators (such as SEEDs), although this might not be advantageous in all cases.

The optical power is supplied to photovoltaic (PV) cells on the back wafer surface. In the implementation shown, the four element, series-connected PV cells are grown in InP, which is a large bandgap semiconductor capable of supplying an open circuit voltage of nearly 4 V. The short wavelength power beam is then fully absorbed by the PV cells, whereas the InP substrate is transparent to the lower energy data beam also incident from the bottom wafer surface. In this manner, the two beams are completely isolated, or "demultiplexed" by the semiconductor substrate material. Interconnection must be accomplished using "vias" to connect these two wafer surfaces.

To demonstrate the concept of optical powering, we recently fabricated an optoelectronic integrated circuit (OEIC) optical logic "smart" pixel array[7,8]. The demonstration circuit (shown in Fig. 5) consists of several transistors, two photoconductors, a laser diode (connected externally) and a four-element PV cell array (fabricated in this case, on the same wafer surface as the logic circuit). Optical data is incident on one of the phototransistors, whereas positive feedback from the laser back to the

circuit is incident via a second phototransistor. The amount of optical feedback is controlled by illuminating one of the photoconductors (PC₁) with a second "control" beam. By this means, the circuit was made to operate variously as a thresholding amplifier (with the control beam power, $P_{\text{control}} = 0$) a bistable switch ($P_{\text{control}} < 560 \mu\text{W}$) and a latch ($P_{\text{control}} > 560 \mu\text{W}$). Illuminating PC₂ when the circuit is latched, turns off the laser. In this mode, the circuit acts as a S-R flip-flop.

Initial results from this smart pixel are given in Table I, along with projected values in the near future, given minor improvements in device performance. These results are, in general, extremely promising. They suggest that such optically powered optical interconnections can, indeed, provide a practical means for achieving a high bandwidth and high density in optical interconnection and computing systems of the future.

This work was also partially funded by a contract from DARPA/RADC.

Table 1

Optically Powered Logic Pixel Performance

Parameter	Meas.	Expected
Gain ($P_{\text{out}}/P_{\text{in}}$)	2.5 - 11	50
Bandwidth (MHz)	40	500
Power Dissipation (mW)	5.3	5
Contrast Ratio	>100	>100
Switching Energy (pJ)	3.8	0.05
Pixel Density ($\#/cm^2$)	300	300

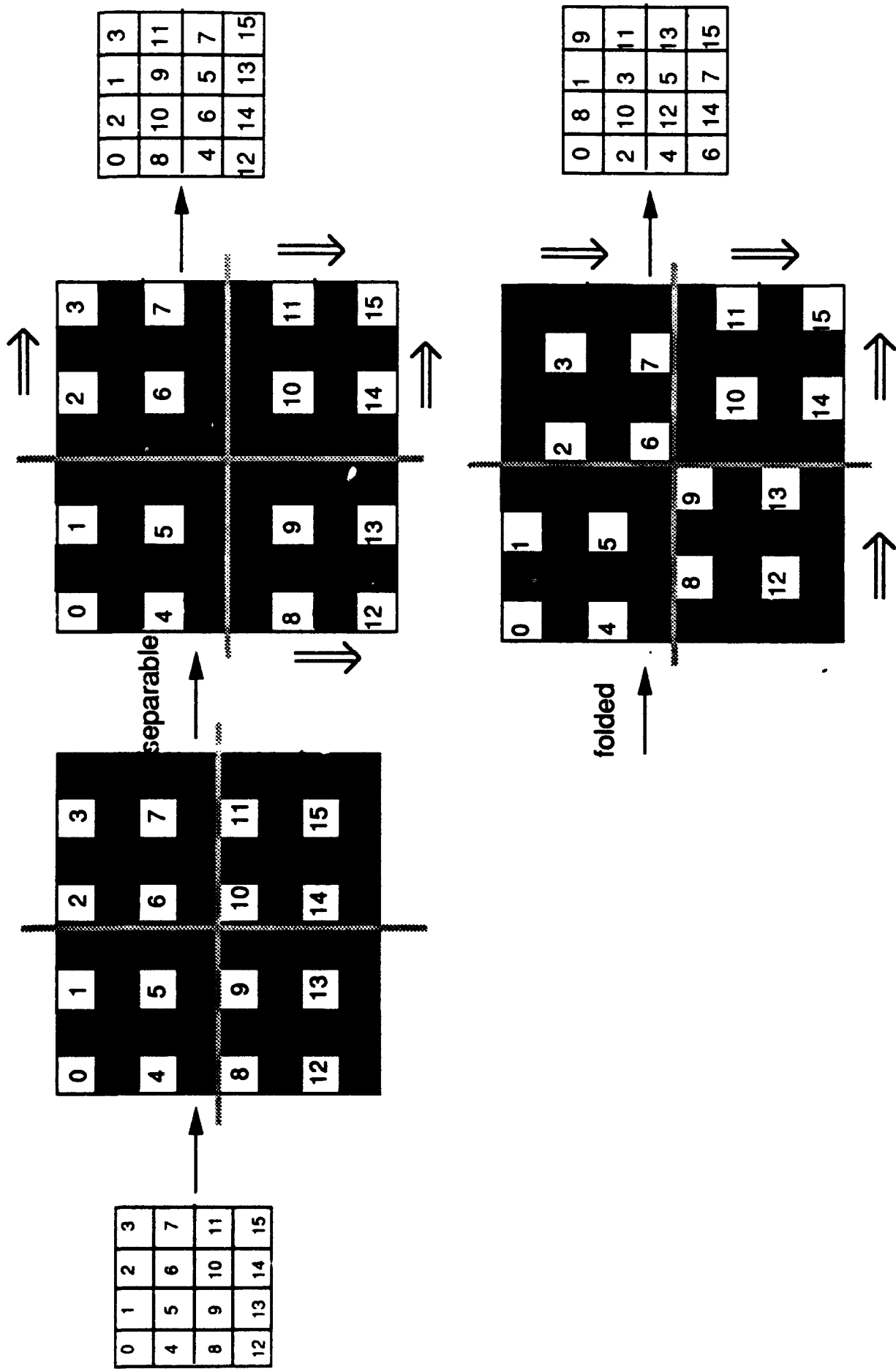


Fig. 1. Schematic representation of the light efficient one-copy shuffle algorithm.

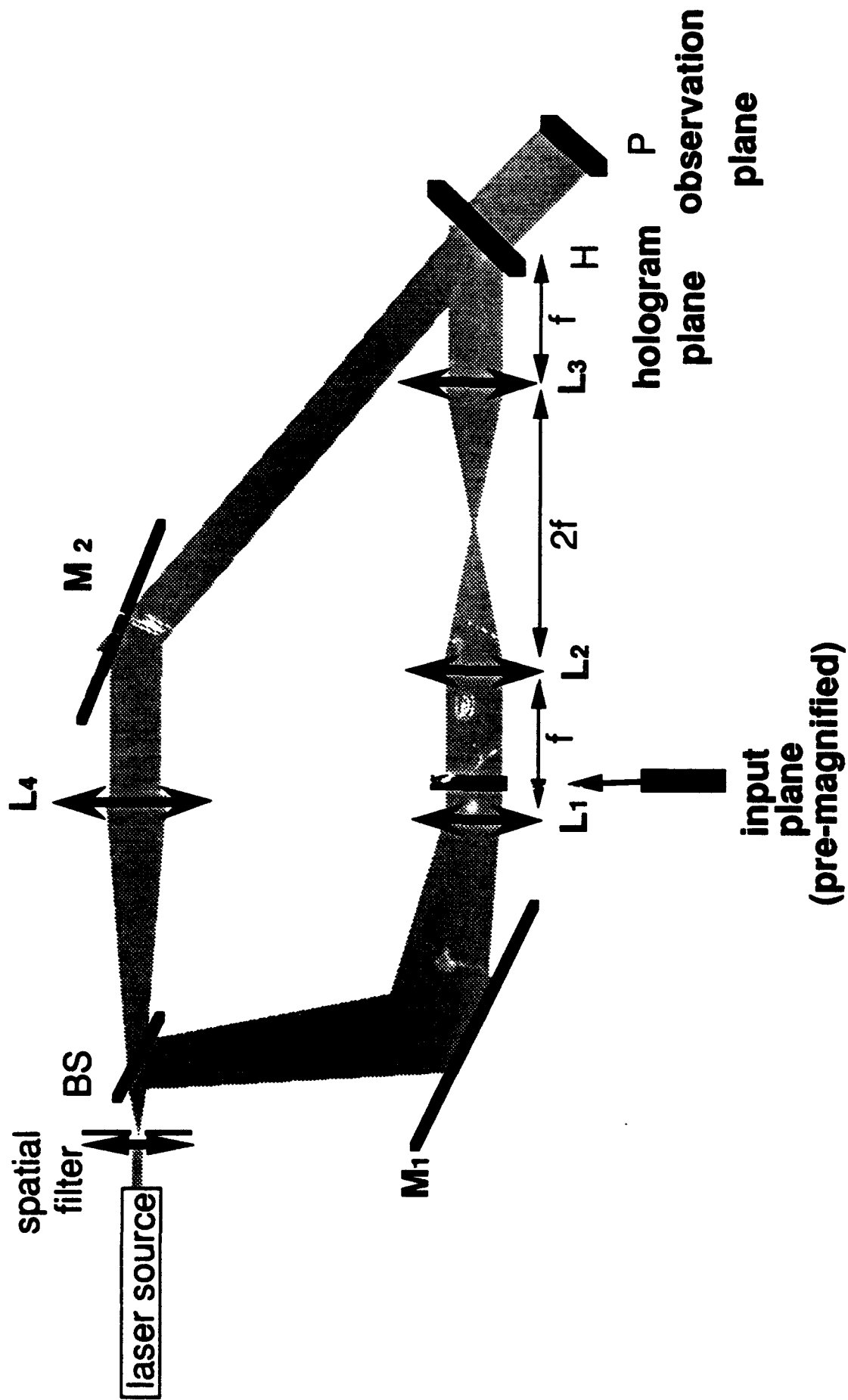


Fig. 2. Experimental setup for making a facet hologram used in the one-copy shuffle algorithm.

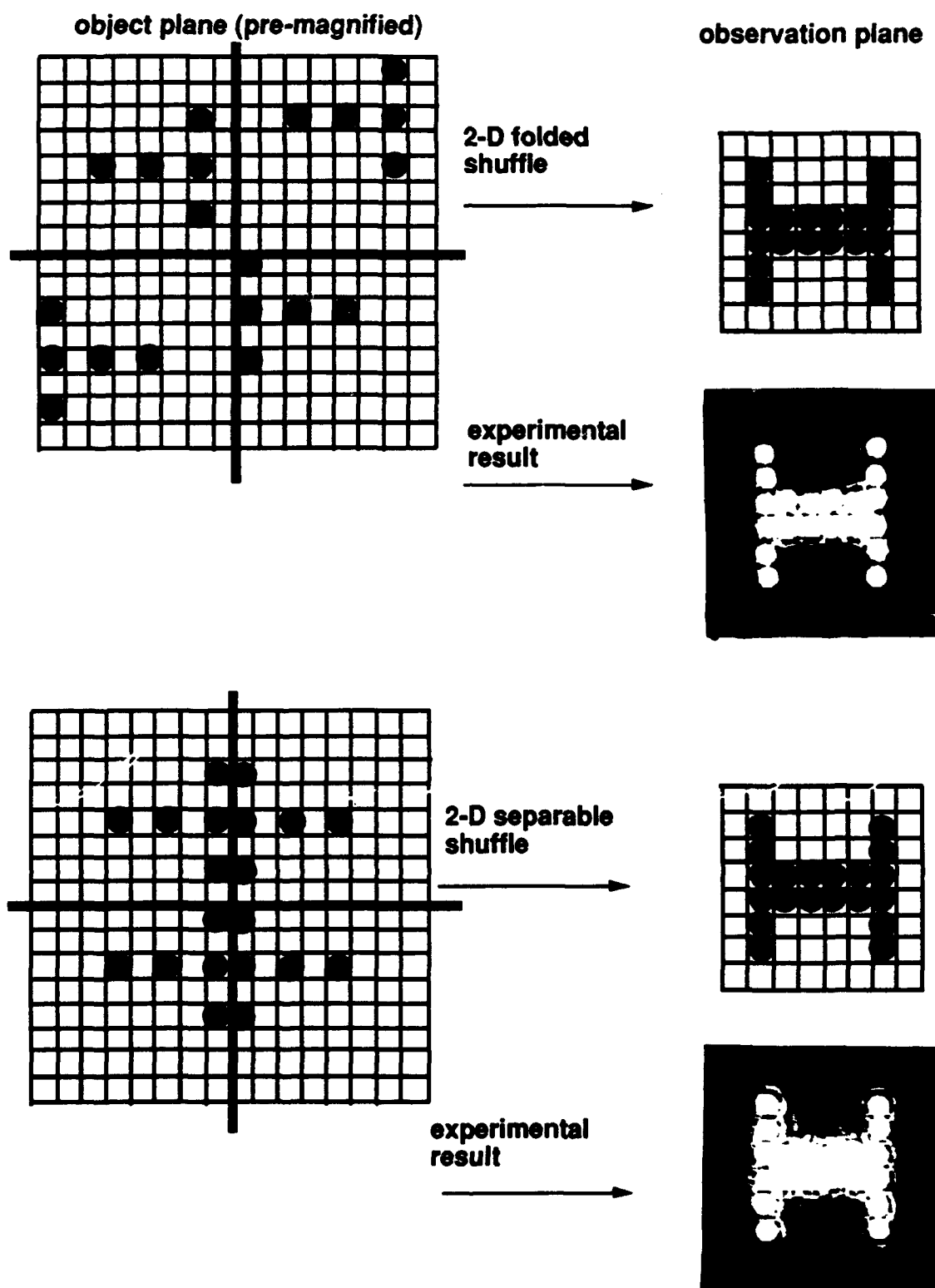


Fig. 3. Simulated and experimental results of the one-copy shuffle algorithm.

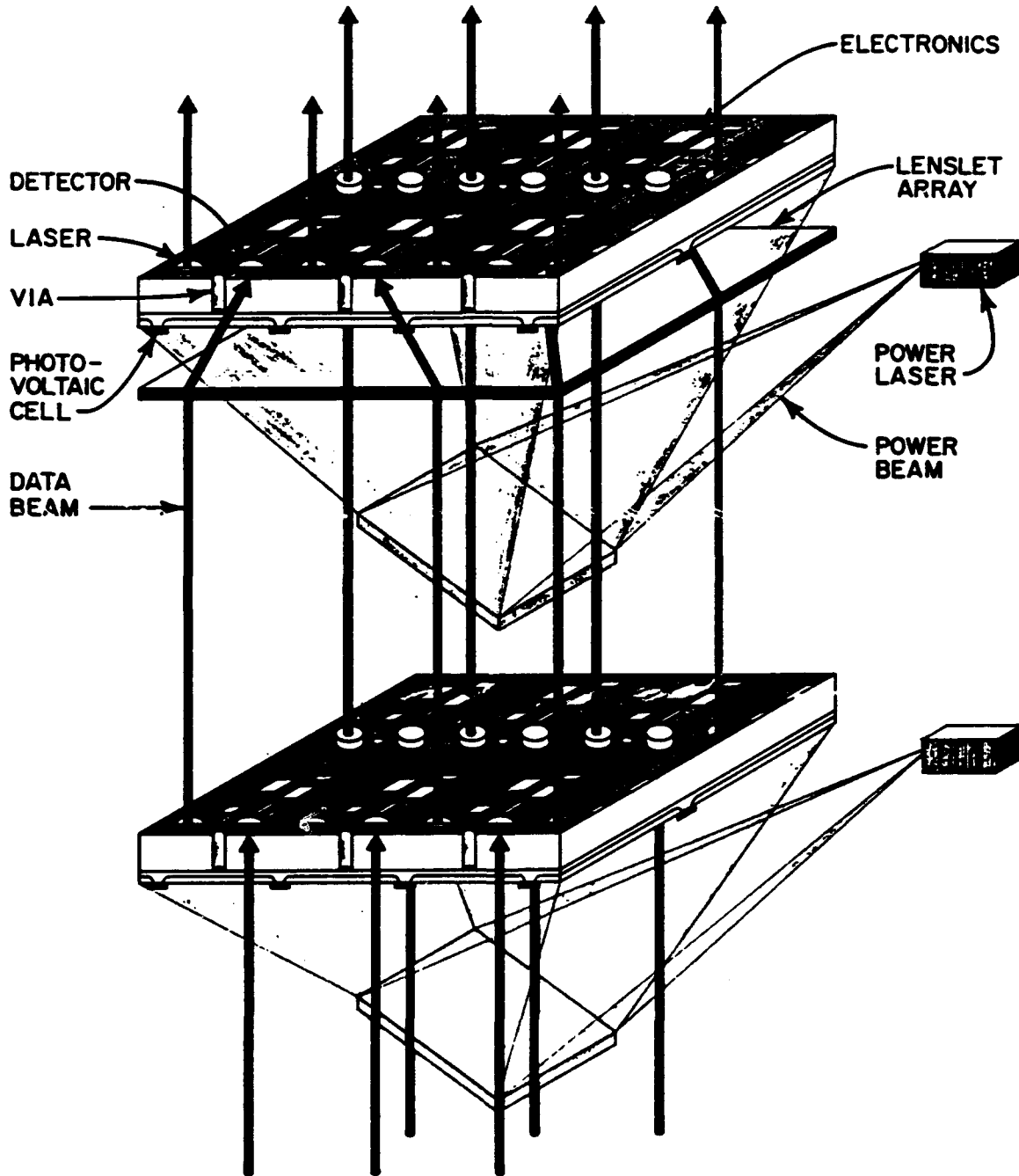


FIG. 4

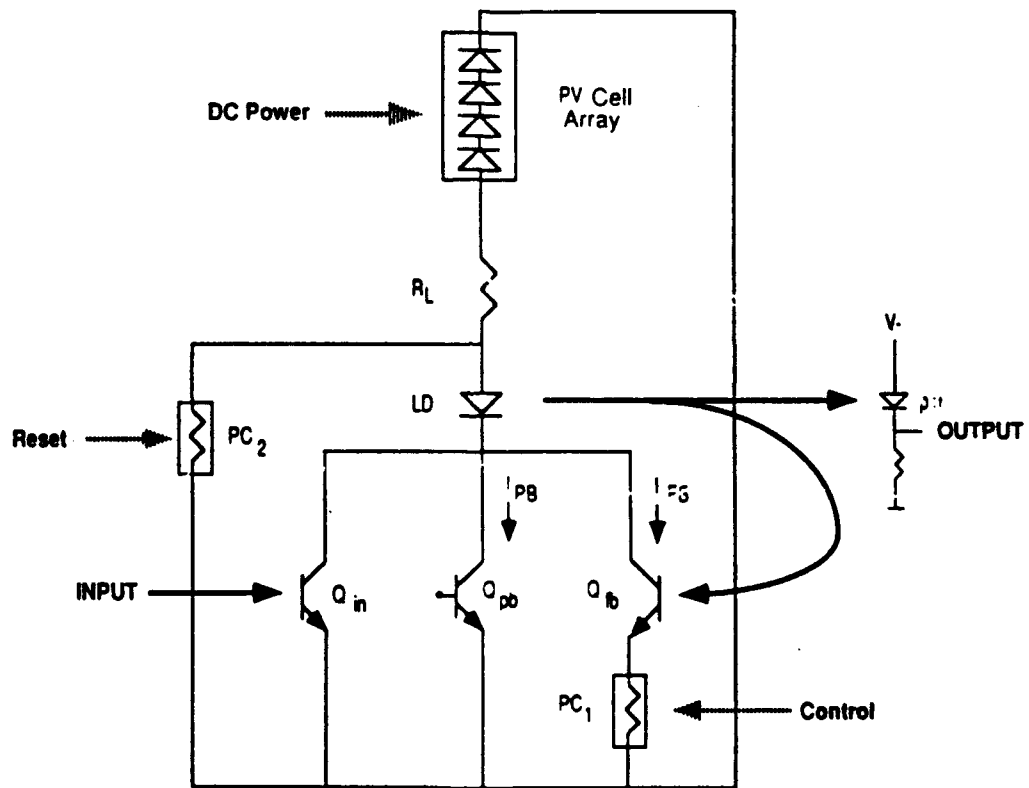


FIG. 5

Interconnections and Spatial Light Modulators for Generalizable Photonic Neural Networks

Armand R. Tanguay, Jr.

The research project described in this report is one of three collaborative efforts incorporated under the task "Generalizable Photonic Neural Networks" within the University Research Initiative "Center for the Integration of Optical Computing". The other two related and complementary research projects are "Architectures for Generalizable Photonic Neural Networks" (Prof. B. Keith Jenkins), and "MBE Growth of Quantum Well Structures for Generalizable Photonic Neural Networks" (Prof. Anupam Madhukar)

The overall goal of these three highly integrated research efforts is the development of a viable, synthetic, and integrated photonic technology for the implementation of low power, compact, massively parallel, generalizable neural network architectures. Such a technology must be manufacturable, flexible in design, and heavily leveraged by related research and development thrusts. Further, the array of chosen components must be inherently compatible and complementary in form and function. To this end, we have addressed during the contract year a number of key research and development issues that will delineate the future impact of photonic neural networks, as outlined below.

The architecture that we are investigating for photonic neural network implementations is shown schematically in Fig. 1. A volume holographic medium is utilized to allow for the required high density of interconnections among the neuron units; this medium may be fixed in the case of a trained network suitable for performing certain tasks based on *a priori* knowledge, or dynamic in the case of a neural network that incorporates a learning algorithm. In order to alleviate several problematic sources of crosstalk and throughput loss that have been characteristic of previously proposed holographic interconnection schemes, a two-dimensional source array of individually coherent but mutually incoherent sources is incorporated to provide for parallel recording of the desired interconnection patterns and weight updates. The corresponding optical system is arranged to transform the spatially distributed source array into sets of angularly multiplexed signal and reference beams that are pairwise coherent, but mutually incoherent to eliminate the potential for coherent recording crosstalk. This double angular multiplexing scheme also eliminates a major source of throughput loss that results from beam degeneracy crosstalk. Two spatial light modulators complete the

architecture, representing the neuron unit outputs (SLM₁) and the neuron unit inputs (SLM₂).

In the recording mode of operation, characteristic for example of a learning or training cycle, the shutter in the upper arm of the architecture is open, and both signal ($\{y_i\}$) and reference (x_j) beams generated by a given source within the source array are incident on the volume holographic recording medium. The simultaneous availability of a coherent source beam from each source provides for a full set of weight updates over all of the input values x_j . In the readout or computational mode of operation, the shutter in the upper arm is closed, and reconstruction of the full set of weighted interconnections is provided by means of the source array in conjunction with SLM₂. Feedback of the reconstructed interconnection matrix to SLM₁ is provided by a combination of mirrors, lenses, and inverting prisms, as shown in Fig. 1. Such feedback can be provided to either the upper arm, the lower arm, or both as demanded by the particular neural network architecture implemented.

During the past year, significant progress has been made in the analysis and quantization of crosstalk and throughput performance achievable in the conventional and incoherent/coherent doubly angularly multiplexed holographic recording and reconstruction schemes, in the analysis and experimental demonstration of the temporal correlation behavior of dynamic (photorefractive crystal) holographic recording media for implementation of dynamic link neural network concepts, in the demonstration of a novel single step copying technique for multiplexed volume holograms that allows for efficient copying of a fully trained set of interconnection holograms, in the implementation and characterization of neuron unit circuitry capable of providing the appropriate optical detection and functional transformation required in each SLM neuron unit, in the analysis of the technological limitations and design considerations that apply to multiple quantum well (MQW) SLM modulator elements, and in the fabrication and characterization of large area hybridization-compatible SLM modulator element arrays that exhibit a relatively high contrast ratio and dynamic range. In addition, we have further developed the high contrast ratio parallel readout capability of optical disc based spatial light modulators for possible incorporation as training pattern generators in such generalizable photonic neural networks. Each of these advances is described in more detail below.

During the contract period, we have extended our preliminary analyses of reconstruction fidelity and optical throughput for the volume holographic interconnection techniques utilized in the double angularly multiplexed and conventional photonic neural network architectures. This has included the use of the optical beam propagation method to numerically model independent interconnection weights and increased numbers of interconnections (compared to our initial modeling studies), as well as the simulation of the subhologram version of the double angularly multiplexed architecture. In addition, we have considered a comprehensive set of recording methods for the conventional interconnection architecture, which has revealed a potentially serious difficulty in the oft-proposed method of using a page-wise sequential recording technique to reduce the influence of cross gratings on the recorded interconnection pattern. This method (in a conventional architecture) requires very large beam ratios between the reference and image beams in order to avoid inadvertent strengthening of the cross gratings. The required beam ratio scales as N^2 for an N-to-N interconnection system, which is impractical for large N.

Sample simulation results based on the optical beam propagation method are shown in Fig. 2 for both the conventional architecture (for several possible recording methods and readout with mutually coherent beams) and the subhologram version of the double angularly multiplexed architecture. In this figure, the RMS error of the diffracted outputs of a ten-to-ten interconnection is shown as a function of the optical throughput, which is defined as the fraction of incident readout light that is diffracted into the desired outputs. The peak throughput achieved for each case occurs at the right-hand end of each curve. As illustrated in the figure, simultaneous recording of each training pair in a conventional architecture results in large fidelity errors in the diffracted outputs due to the occurrence of extraneous cross gratings. Reduction or elimination of these cross gratings using page-wise sequential or fully sequential recording techniques can improve reconstruction fidelity (and peak throughput), but at the cost of a significantly larger number of exposures to achieve the desired interconnections. For example, fully sequential recording results in good reconstruction fidelity (as shown in Fig. 2), but requires N^2 more exposures than simultaneous recording. The double angularly multiplexed architecture, however, achieves comparable reconstruction fidelity to sequential recording in a conventional architecture while requiring only one exposure for each training pair. Low interchannel crosstalk is therefore achievable while taking full advantage of the parallelism inherent in optical interconnections to perform the requisite weight updates in adaptive neural networks.

One of the advanced neural network algorithms that we are investigating for implementation in a modified version of the double angularly multiplexed architecture is based on the dynamic link concepts proposed by Prof. Christoph von der Malsburg (Depts. of Computer Science and Electrical Engineering-Systems at USC). A key feature of the dynamic link architecture is the formation of interconnection weights based on the temporal correlation between time varying neuron unit outputs. We have investigated the use of photorefractive media as interconnection elements in which the interconnection weights are related to the *correlations* among pairs of time-varying grating writing beams. Using a charge transport model of photorefractive grating formation, we have obtained analytic solutions for the effective modulation depth of gratings written in the low modulation depth regime, and numerical solutions when the modulation depth is large. Excellent agreement between these solutions and experiments using single crystal bismuth silicon oxide ($\text{Bi}_{12}\text{SiO}_{20}$) have been obtained. By utilizing the large temporal bandwidths available in our hybrid-integrated SLM arrays and incorporating photorefractive correlating interconnection elements, very high processing throughput for photonic implementations of the dynamic link architecture may be achievable.

One of the most significant problems inherent in neural network implementations has been the difficulty involved in copying a learned interconnection pattern from a master interconnection to one or more identical copies. This capability is essential for both military and commercial viability of any but the simplest neural network implementations, as the training sequence can in many cases prove to be the rate limiting step. In addition, the weights that result from a particular learning sequence may not be known, and in the case of large scale networks, may not prove measurable in finite time if at all. We have shown that the doubly angularly multiplexed, incoherent/coherent recording and reconstruction geometry for incorporation of holographic interconnection weights is uniquely suited to a single step copying process that allows for reproduction of a fully multiplexed master hologram. Recently, single step copying of multiplexed volume holograms has been demonstrated experimentally in collaboration with Prof. Jenkins' research group. In these experiments, three superposed holograms (each of a single letter) were successfully copied from a master hologram implemented in DuPont's Omnidex photopolymer material to a second photopolymer copy hologram in a single recording step.

During the contract period, we have invented a novel hybrid spatial light modulator configuration that allows for *face-to-face* contact by flip-chip bonding techniques between a silicon chip that incorporates dual channel detectors and control electronics that implement a dual channel sigmoidal transfer function, and a compound semiconductor chip that incorporates an array of multiple quantum well spatial light modulation elements. By utilizing standard CAD design tools and SPICE circuit simulations, we have designed and evaluated appropriate silicon CMOS circuitry using the 2 μm design rules allowed within the MOSIS CMOS design repertoire. To date, functional 6 x 6 arrays of 100 μm square pixels have been successfully fabricated and evaluated that exhibit a high degree of transfer function uniformity across the array. Operational bandwidths in excess of 4 MHz (large signal) and 14 MHz (small signal) have been successfully demonstrated. A new circuit is currently being designed with projected 20 nsec rise and fall times. It will accommodate the 0.5 Volt input signal generated by the integrated optical detectors and is designed to operate with an increased output voltage swing of 10 Volts, which is compatible with the drive requirements of the multiple quantum well compound semiconductor spatial light modulators discussed below.

Extensive analyses of multiple quantum well based spatial light modulation elements have been undertaken to establish the technological limitations and design constraints characteristic of the asymmetric Fabry-Perot optical cavity geometry, which is often employed to enhance both the contrast ratio and dynamic range of thin MQW modulator structures. These analyses have pointed out the exceptionally high degree of growth thickness uniformity required both within the multiple quantum well region itself, as well as in the incorporated Bragg mirrors that comprise the Fabry-Perot cavity. In these studies, the material systems investigated have included both AlGaAs/GaAs and strained layer InGaAs/GaAs, with the latter system of particular interest due to its capability for growth on a *transparent* GaAs substrate. Such a structure is highly desirable for incorporation in a flip-chip bonded hybrid Si/GaAs spatial light modulator structure, as described above. In collaboration with Prof. Madhukar's research group, large area arrays of InGaAs/GaAs multiple quantum well structures have been fabricated in asymmetric Fabry-Perot cavities by molecular beam epitaxial (MBE) growth techniques, resulting in contrast ratios as high as 66:1 with a dynamic range of 30%. In addition, an *inverted* asymmetric Fabry-Perot cavity multiple quantum well modulator has been fabricated and evaluated that exhibits a contrast ratio of 12:1 and a dynamic range of 20% at 9565 \AA . In this novel structure, the *low* reflectivity Bragg mirror is grown first, followed by the multiple quantum well region. An externally deposited high reflectivity dielectric mirror

completes the cavity, reducing the total MBE growth time significantly while allowing for *ex situ* post-growth tuning of the cavity resonance.

Finally, we have utilized a novel differential interferometric readout technique to allow parallel access to 1 cm² images written directly onto optical disc media by area encoding techniques, with image sizes of 512 x 512 superpixels and an enhanced output contrast ratio of up to 100:1. This achievement has been made possible by the use of glass (as opposed to polycarbonate) optical disc substrates, as well as by the development (in conjunction with Apex Systems, Inc. in Boulder, Colorado) of a novel optical disc media tester that allows for submicron positioning accuracy of each subpixel bit over very large areas on the optical disc. Using this optical media tester, we have successfully recorded and read out complex pictorial gray scale images with excellent image fidelity and throughput linearity. Throughput linearity has been examined both experimentally by recording patterns with different duty cycles within each superpixel, and theoretically by utilization of an angular spectrum decomposition method. Incorporation of the rotational motion characteristic of optical disc drives allows for the high speed presentation of very large numbers of training images to a neural network. Further applications of this emerging technology to neural network systems are under continuing investigation.

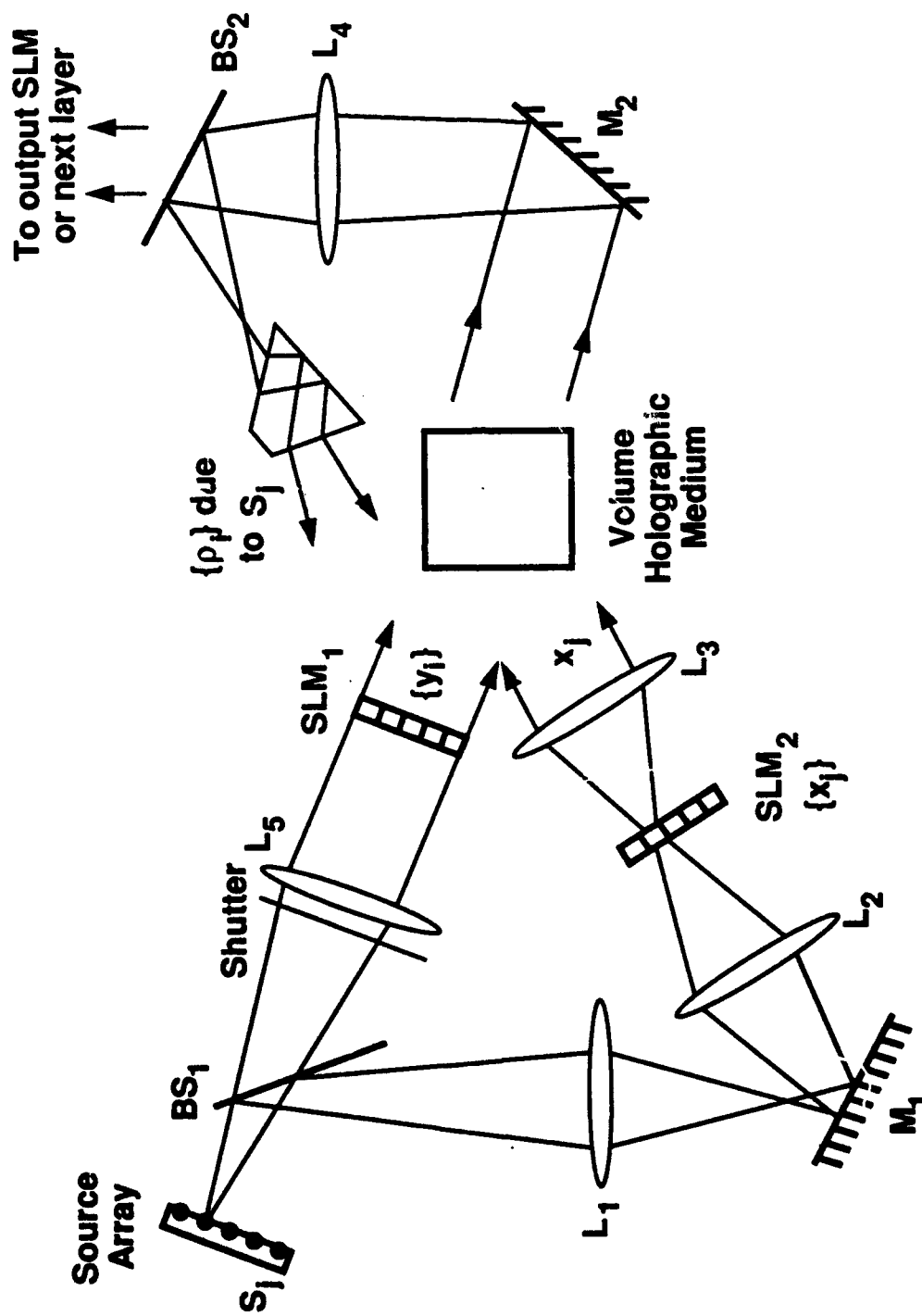


Fig. 1 Schematic diagram of a generalizable photonic neural network architecture, incorporating incoherent/coherent and doubly angularly multiplexed holographic interconnections, an array of individually coherent but mutually incoherent sources, and spatial light modulators that contain the neuron unit arrays.

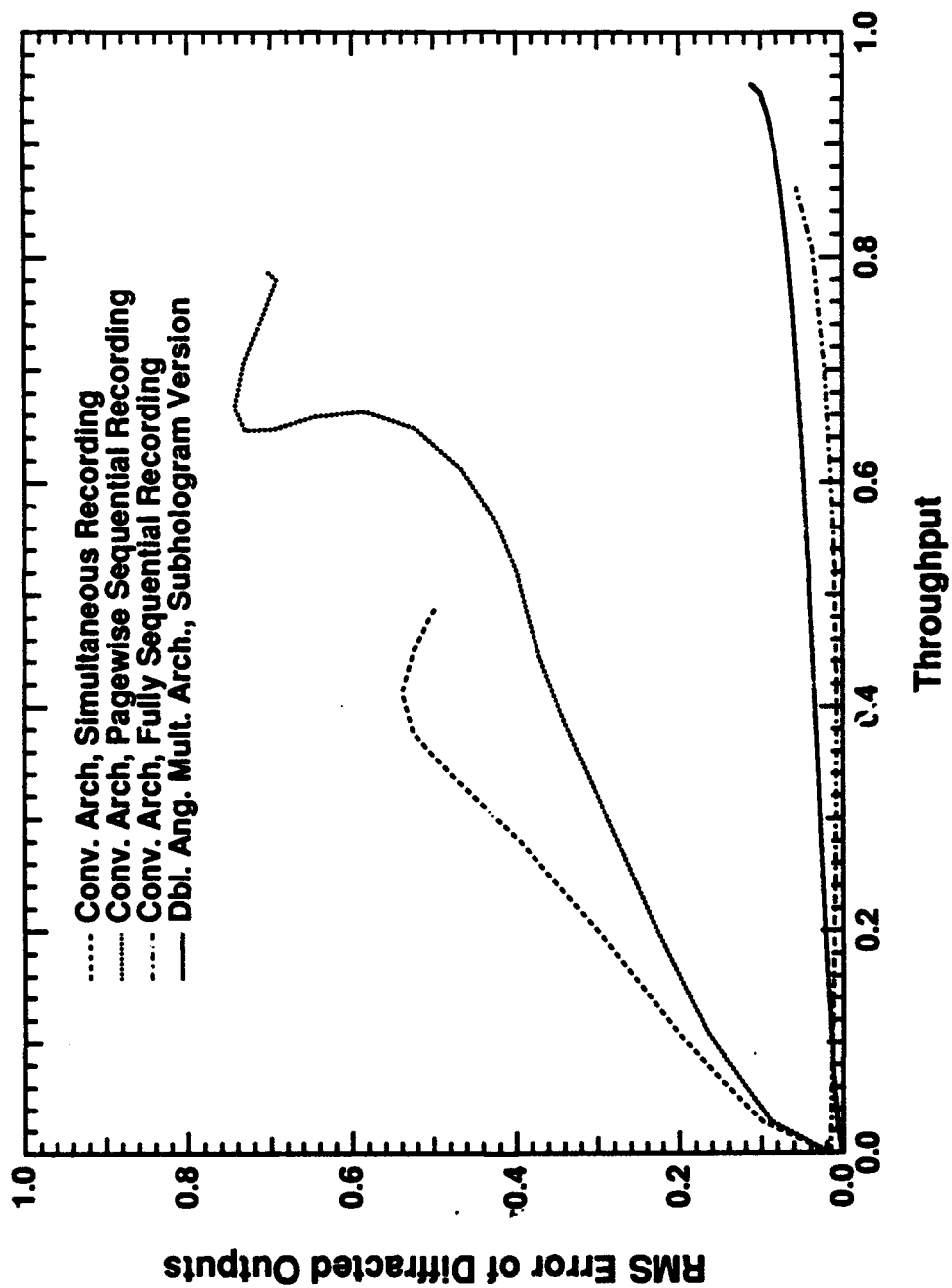


Fig. 2 RMS error of diffracted outputs as a function of optical throughput for the conventional architecture (using several recording methods) and the subhologram version of the double angularly multiplexed architecture. Beam ratios of 100:1 are assumed for both the conventional architecture using the page-wise sequential recording method and the subhologram version of the double angularly multiplexed architecture.

MBE Growth of Quantum Well Structures for Generalizable Photonic Neural Networks

A. Madhukar

During this reporting period the following major advances in the realization and use of strained InGaAs / GaAs multiple quantum well (MQW) based asymmetric Fabry-Perot (ASFP) spatial light modulators (SLM) were made;

1. Realization of the first *inverted* cavity ASFP modulators:

To take advantage of the transparency of the GaAs substrate which affords flip-chip bonding of the InGaAs / GaAs based SLM and a Si chip containing the control electronics, we designed and realized the first *inverted* cavity p-i (MQW)-n modulator in which incident light passes through the (antireflection coated) substrate as shown in the inset of Fig. 1. The reflectivity as a function of wavelength (Fig. 1) gave a typical contrast ratio of 12:1 at the Fabry-Perot wavelength for an applied bias of -16 V. Details are given in publication number 1. Work on realization of up to 10 X 10 arrays of 50 X 50 μm^2 pixels with uniformity in the device characteristics is continuing.

2. Realization of the first vertically integrated p-i(MQW)-n modulator and heterojunction phototransistor to obtain optically controlled SLM:

While continuing our work on the electrically addressable SLMs, during this reporting period we initiated examination of several options for realizing optically controlled modulators and implemented a design based on vertically integrated emitter-down heterojunction phototransistor and p-i(MQW)-n *inverted* cavity modulator (Fig.2a). The modulator reflectivity at zero and 0.3mW input light power are shown in Fig. 2b. A contrast ratio of 12:1 with a reflectivity change of 27% at the Fabry-Perot wavelength of 9708Å is observed. Details are given in publication number 2. Work on improved device performance and on extending the operating wavelength to 0.98 μm (through increased In content in the InGaAs / GaAs MQW) is continuing.

3. ASFP-SLM based digital optical switches:

The p-i(MQW)-n configuration ASFP modulator structures grown were examined for their performance in a wide variety of digital optical switches. Particular emphasis was laid on the use of *inverted* cavity design which permits the read and write light beams to impinge from opposite sides, thus reducing many growth / regrowth and processing considerations otherwise motivated by the need for optical isolation. The following types of switches were implemented;

- (a) Self electro-optic effect device (SEED) based on blue-shift of the *inverted* cavity ASFP modulator Fabry-Perot mode:

As opposed to the conventional usage of the exciton red-shift, we implemented a new class of SEED device based upon the blue shift of the Fabry-Perot mode in "normally-off" InGaAs / GaAs ASFP modulators. The SEEDs examined included diode-SEED, transistor-SEED, phototransistor-SEED, and the symmetric-SEED. While the details of the first three can be found in publication number 3, we note here the behavior of the symmetric-SEED. A contrast ratio of 5:1 was realized in the strained InGaAs /GaAs system. This is comparable to the best GaAs / AlGaAs based symmetric-SEEDs. Details are given in publication number 4.

- (b) Monolithic Opto-Electronic Transistor (MOET):

The MOET is based upon the usage of the negative differential resistance (NDR) of a resonant tunneling diode (RTD) to achieve bistability. A schematic of the circuit is shown in Fig. 3a. The InGaAs / GaAs MQW based p-i(MQW)-n ASFP modulator /detector pixels of the structures grown as part of the effort under item 1 above were thus combined with InGaAs /AlAs / GaAs based RTD's grown under the JSEP program to examine MOET performance. For amplification of the RTD signal, different types of FETs were used. While the details of these different implementations may be found in publication number 4, here we show in Fig.3b the MOET characteristics obtained when a GaAs MESFET(grown, fabricated, and tested under the sponsorship of JSEP) is used in the circuit. A contrast ratio of 4.5:1 and a reflectivity change of 35% with a fan-out of 2 is obtained. The inherent contrast of the modulator is significantly higher (~20:1) at the 0.8mW bias light power employed when ~15V reverse bias is applied. The lower value of 4.5:1 obtained for the MOET is due to the fact that GaAs MESFET used had a 12V source-drain breakdown voltage and could therefore provide a maximum of ~12V drop across the modulator pixel. Details may be found in publication number 5.

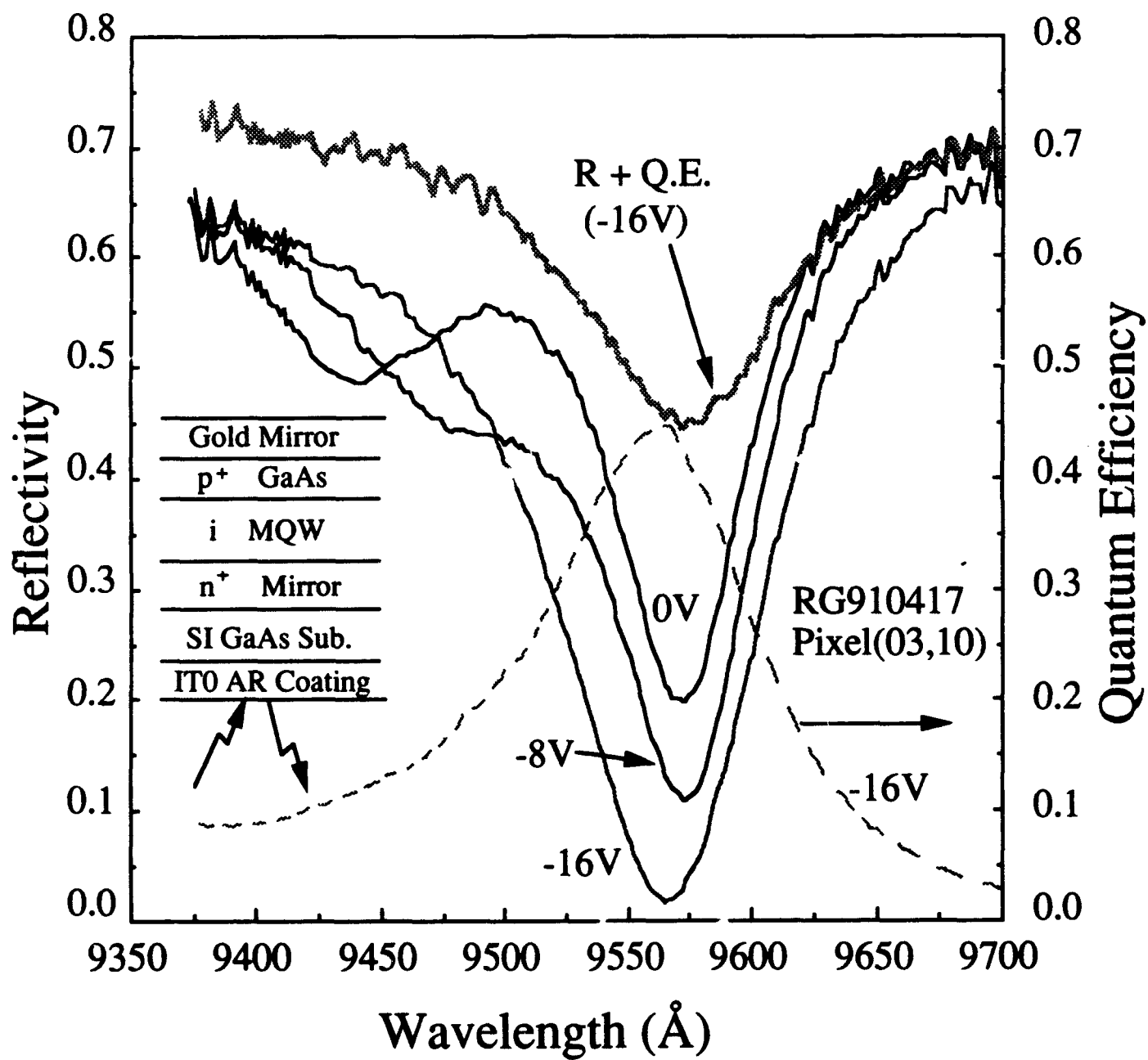


Figure 1

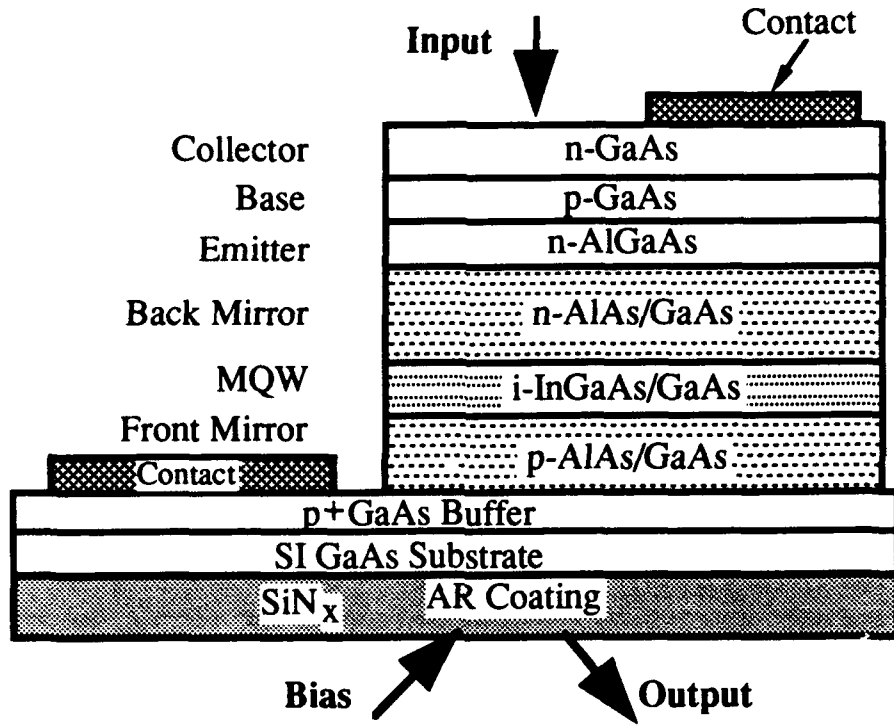


Figure 2a

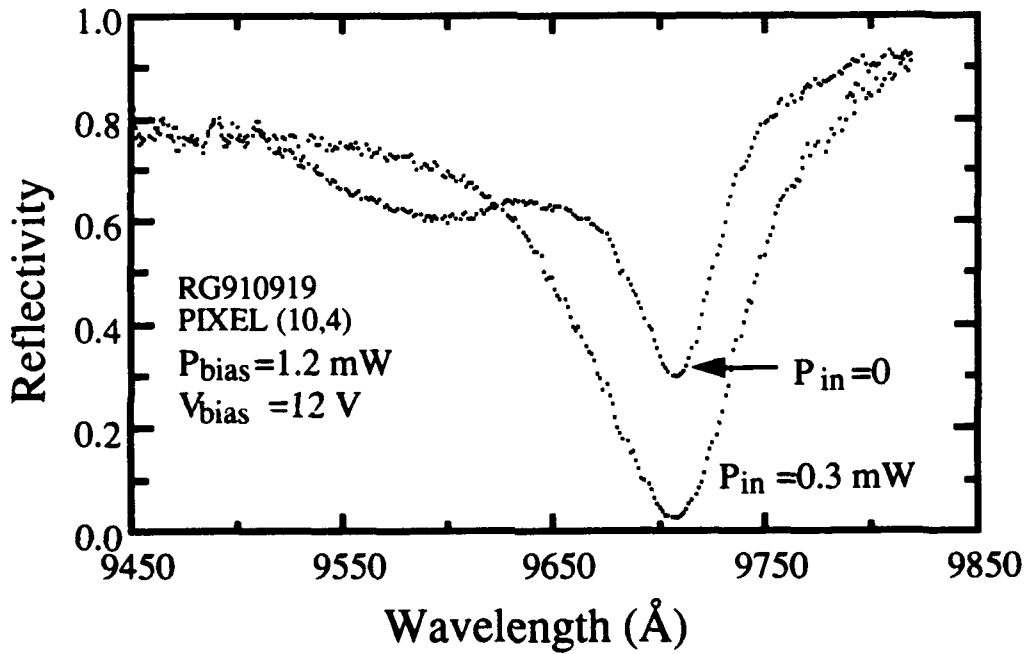


Figure 2b

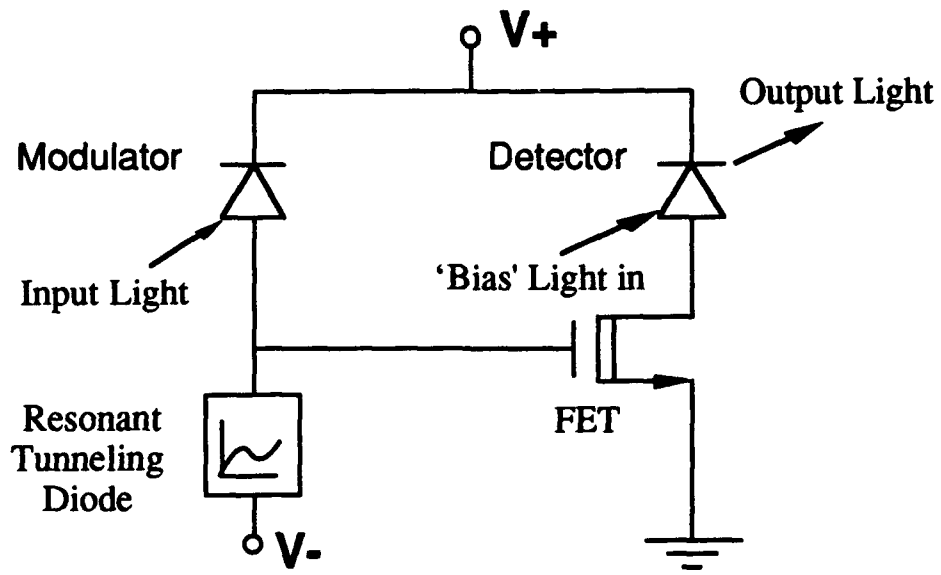


Figure 3a

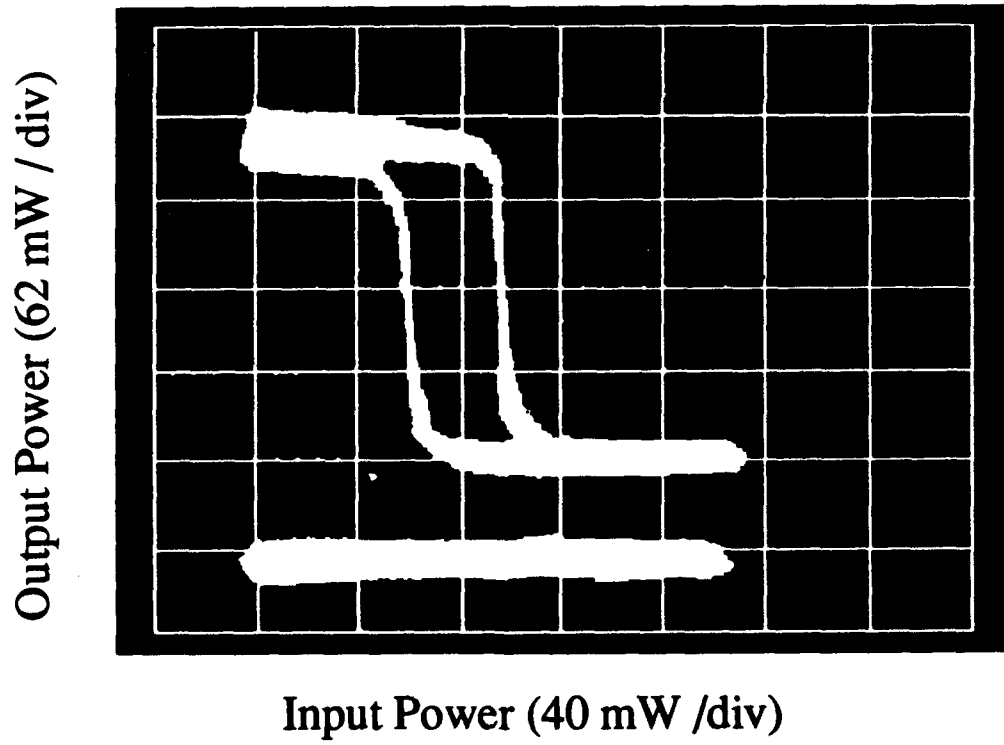


Figure 3b

Cloning Of Generalizable Photonic Neural Network Interconnections

B. Keith Jenkins

The joint effort among B. Keith Jenkins, Anupam Madhukar, and Armand R. Tanguay, Jr. on the photonic implementation of generalizable neural networks has progressed rapidly during the past year of the URI program. A key novel feature of our approach is the fast duplication capability of the volume interconnection element. This feature enables the production *en masse* of photonic neural networks that utilize pre-trained synaptic interconnections implemented in a volume holographic element. This is a critical capability for large-scale photonic neural networks because training the network to learn a given processing function may entail a large overhead in both hardware complexity and processing (learning) time, particularly in the case of multilayer networks. An attractive paradigm is to train only a "master" network, and then insert duplicates of its interconnection hologram(s) into simpler and faster processors. This copying capability can also be used for multiplexed volume holographic optical elements, and thus potentially improves the manufacturability of such optical elements.

Extension of previously reported hologram copying techniques [1] to multiplexed volume holograms typically requires a sequential set of exposures to avoid creating significant crosstalk and to maintain independence of each multiplexed hologram. Typically, such a procedure requires complicated exposure schedules and yields results that lack repeatability. In order to overcome these drawbacks, we are developing a hologram copying process that can be performed in a single step without inducing crosstalk. In the remainder of this Letter, the term *hologram* will refer to one independent hologram or holographic grating, a set of which may be multiplexed in one *holographic element*, such that the individual holograms may be spatially superimposed in a common region within the volume holographic medium.

The copying process described herein assumes only that the master holographic element can be reconstructed with angularly multiplexed reference beams that are separated in angle by more than the angular sensitivity of the holograms; that each hologram reconstructs its corresponding wavefront independently of the other holograms and is intended to likewise remain independent in the copy; and that the relative phases among the set of holograms are not of concern. The master holographic element may be generated by a set of sequential exposures, or

by a single simultaneous exposure as described below [2, 3, 4, 5]. The copying technique utilizes a set of individually coherent sources that are mutually incoherent. Each source is used to generate two reference beams, one at the master holographic element and one at the copy holographic medium; the reconstructed object beam from the master interferes with the reference beam at the copy to record a hologram. By turning on all sources simultaneously, their mutual incoherence prevents the recording of undesired cross-coupling gratings, and therefore independence of the different holograms is maintained in a single-step exposure.

Figure 1 shows the architecture that provides for single-step copying. A set of individually coherent but mutually incoherent sources is used to generate a set of reference beams. Each such beam is intended to duplicate, at the master holographic element, the angle, location, and phasefront of the corresponding reference beam that was used to expose the master holographic element. For cases in which the reference beams are incident in a regular angularly multiplexed geometry, a regular 1-D or 2-D spatial array of sources can generate the beams. Such an array of mutually incoherent sources can be either fabricated [6] or generated from a single coherent source and an optical system [5]. In the architecture shown, the reference beams illuminate the primary (master) holographic element simultaneously, recalling all of the stored holograms in parallel. The source array is imaged so that it generates a set of individually identical reference beam phasefronts on the secondary (copy) holographic medium. In Fig. 1, the reference beam phasefronts in planes P₁ and P₂ are identical. Similarly, the reconstructed object beams are also imaged in amplitude and phase onto the secondary medium. The appropriate pairs of beams interfere in the secondary holographic medium, making a complete copy of the original multiplexed hologram.

Note two aspects of this copying technique. First, it is the mutual incoherence of sources that permits the copy process to be performed in a single exposure step. Second, the relative phases among the different holograms can in principle also be preserved in the copy by using a sufficiently stable and aberration-free optical system. However, in this report we consider only systems and applications in which these relative phases are not of concern.

In a preliminary demonstration of this concept, a master holographic element was first exposed, consisting of three holograms that were angularly multiplexed on the same region of a dichromated gelatin holographic plate. Each hologram consists of a volume grating and was exposed by interfering two uniform, collimated beams. The path length

difference between any two of these beams (measured from the source to the holographic plate) was much greater than the coherence length. Each beam was then split into separate reference beam and object beam paths. The six beams were then incident (each at a different angle) on the same region of the holographic plate, where they recorded three independent holographic gratings. This technique records multiplexed holograms that can be recalled independently, and has been described and studied for use in neural network interconnections [2, 3, 4].

In the copying architecture, a similar set of reference beams illuminates the master holographic element, and reconstructs the three object beams. A three lens system images the amplitude and phasefront of each reconstructed object beam onto the copy holographic medium. A dichromated gelatin plate was used for the copy medium. Beamsplitters provide duplicates of the master reference beams at the copy holographic medium; the optical path lengths are kept equal, pairwise, to insure mutual coherence between each object beam and its corresponding reference beam at the copy.

Figure 2 shows the object beams reconstructed from a master holographic element and its copy. The copy was made in a single exposure. The reconstructions shown in Fig. 2a and 2b were obtained by placing the holographic plates of first the master (Fig. 2a) and then the copy (Fig. 2b) in a reconstruction setup. Measured diffraction efficiencies were: master hologram: 20.5 % (A), 23.6 % (B), and 20.3 % (C); copy hologram: 23.3 ± 0.9 % (A), 19.3 ± 0.9 % (B), and 17.5 ± 1.3 % (C). Each diffraction efficiency of the copy is given by the mean and standard deviation over four separate copying experiments. In Fig. 2c, one of the reference beams has been blocked; the independence of reconstructions from the copy is demonstrated by the absence of the corresponding reconstructed beam. In fact, the measured crosstalk was on the order of 10^{-4} at 15 cm behind the holographic plate.

Several factors can provide bounds on the scalability and applicability of this copying process. For example, the available dynamic range of a given recording material forces a trade-off between achievable diffraction efficiency and the number of holograms that are spatially superimposed. This tradeoff manifests itself differently in distinct classes of materials because of different functional responses of the modulation index to the recording intensity pattern. The f-number and space-bandwidth product (SBWP) of the lenses used to relay the information from the master hologram to the copy hologram imposes an upper limit on the number of holograms together with the allowable complexity of each

hologram. Phase aberrations of the relay lenses, and nonlinearities in the recording and reconstruction process, can also affect the quality of the hologram copies. Often, the intended end use of the holographic element will dictate limitations that may be more or less restrictive than those imposed by the copying system; as a result, in some cases the copying system limitations (particularly those due to the relay lenses) will not be of concern.

Careful design of the master holographic element may well circumvent many of the potential limitations outlined above. For example, as part of our joint effort we have been studying the photonic neural network architecture that utilizes incoherent/coherent holographic interconnections and double angular multiplexing [2, 3, 4]. The reconstructed object beams in the holographic interconnections employed in this neural network architecture are partially overlapping in angle as well as in space. In the duplication of this type of interconnection, the f-number and SBWP limitations of the lens relay optics of the copying system, as well as the holographic material dynamic range limitations, are significantly reduced. As this example indicates, the eventual manufacturability of a given holographic element can be anticipated in its design, and in the design of the master recording architecture, by incorporating any limitations implied by the envisioned copying technique.

Extensions of the system to allow for the generation of non-identical copies are also possible. For example, additional holograms can be added in conjunction with those copied from the master; the nature of the reference beams at the copy can be different from those of the master if desired; in some cases filtering can be performed on the object beam path from the master to the copy to decrease noise; magnification can potentially be inserted between the master and the copy; and the relative diffraction efficiencies can be changed by altering either each beam-pair ratio or each beam intensity.

References

1. V. A. Vanin, *Sov. J. Quantum Electron.* 8(7), 809-818 (1978).
2. B. K. Jenkins, G. C. Petrisor, S. Piazzolla, P. Asthana, and A. R. Tanguay, Jr, *Conference Record*, 1990 International Topical Meeting On Optical Computing, SPIE 1359, 317-318 (April 1990).

3. B. K. Jenkins and A. R. Tanguay, Jr., in *Neural Networks for Signal Processing*, B. Kosko, ed. (Prentice-Hall, Englewood Cliffs, NJ, 1992) Chap. 9, pp. 287-382.
4. P. Asthana, G. Nordin, S. Piazzolla, A. R. Tanguay, Jr., and B. K. Jenkins, *Technical Digest*, OSA Annual Meeting, paper FK6, p. 242 (Nov 1990).
5. J. Hong and P. Yeh, *Technical Digest*, Optical Computing Topical Meeting (Optical Society of America, Washington, D.C., March 1991) pp. 160-164.
6. J. L. Jewell, J. P. Harbison, A. Scherer, Y. H. Lee, and L. T. Florez, *IEEE J. Quantum Electronics* 27(6), 1332-1346 (1991).

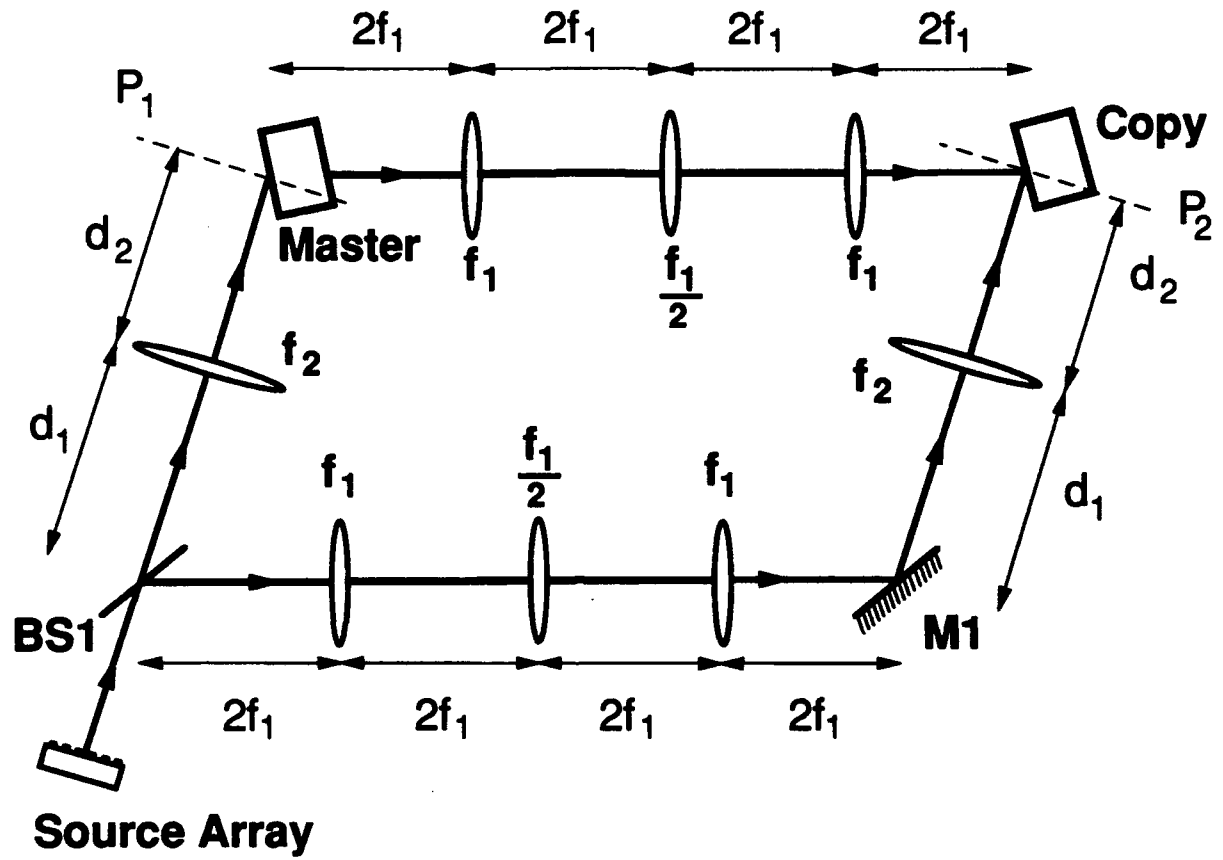


Fig. 1. Optical system for single-step copying of a multiplexed volume holographic element.

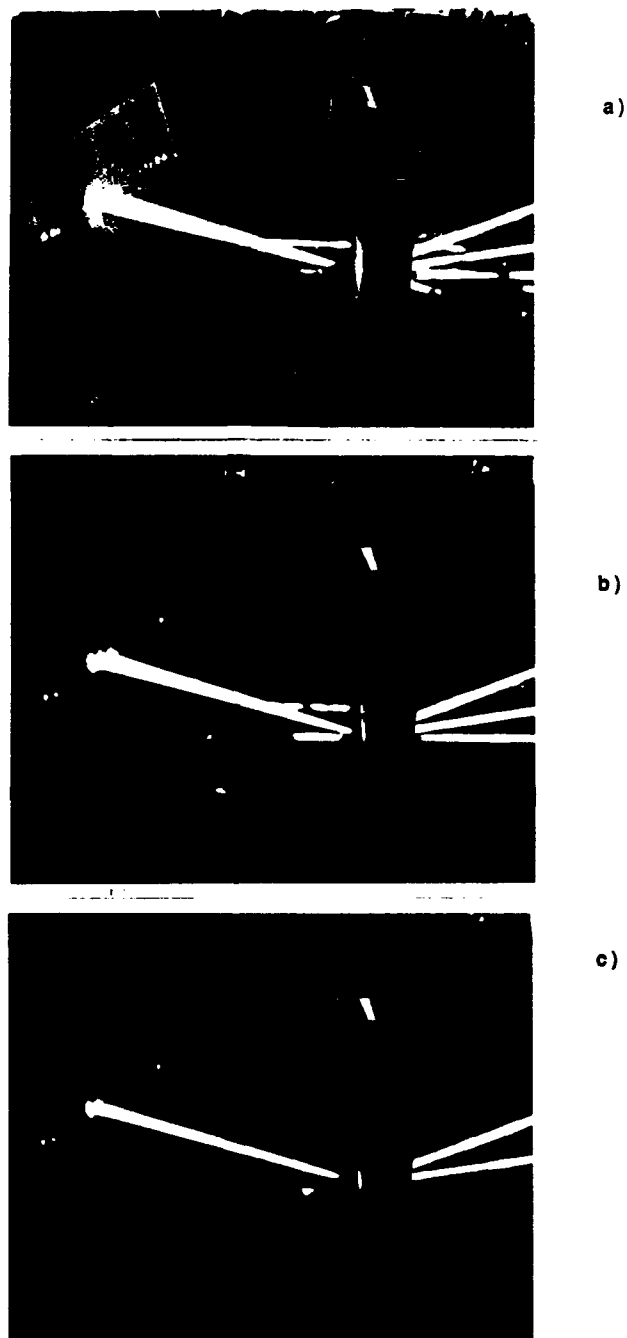


Fig. 2. Experimental reconstruction of object beams obtained first from the master holographic element and then from its copy, using the same set up, showing: (a) the master hologram reconstructing the three object beams; (b) the copy hologram reconstructing the three object beams; (c) demonstration of absence of crosstalk gratings in the copy by showing two reference beams reconstructing only the two corresponding object beams.

Ultralow Threshold Laser Array Elements

P. Daniel Dapkus

Surface emitting lasers utilizing strained InGaAs/GaAs quantum wells are of great relevance for many applications in optical computing where low threshold and high efficiency are basic requirements for large scale integration. In this report, we present an overview of the progress in our research during the last year towards the fabrication of ultra-low-threshold surface emitting lasers. The first step towards the development of the surface emitting laser was to optimize the MOCVD growth conditions for a high quality active region material. In order to evaluate the material, broad area lasers (100mm stripes) employing single In_{0.2}Ga_{0.8}As/GaAs strain quantum well and GRINCH confinement between the Al_{0.5}Ga_{0.5}As cladding and the well barrier were fabricated. The optimization of the growth conditions is done after the results of the characterization of these lasers. Uniform low threshold current was observed with current density as low as 135 A/cm² for a 1.0mm cavity length for lasers emitting at 1 mm with 80% external efficiency. From the dependence of the external efficiency on the cavity length, we estimate the internal quantum efficiency and internal losses to be 0.9 and 3.2 cm⁻¹ respectively.

The reproducible growth of Bragg reflectors by MOCVD was also strongly emphasized. Since, in vertical cavity surface emitting laser, the gain path is limited to the quantum well length (approximately 90 Å), small variations in reflectivity have strong consequences on the laser performance. Besides the absolute value of the reflectivity, the spectral positioning of the high reflectivity band of the Bragg mirror has to be controlled for the resonance of the Fabry-Perot cavity to match the quantum well emission. In either case, the control of the layer thicknesses is crucial. An in-situ technique based on laser reflectometry was developed to correct any run-to-run growth rate variation (1). Before the growth of the GaAs and AlAs mirror layers, thicker buffer layers of these materials are grown at the same conditions of the mirror growth. At this time the reflectivity oscillations are measured and the growth rate determined. The growth is interrupted momentarily to allow for an update of the mirror layers' times in the control program and the growth is then restarted. Good control of the thickness was provided by this technique and laser structures for vertical cavity surface emitting laser processing were obtained.

In our approach for the vertical cavity surface emitting laser the current injection is done parallel to the well such that all the carrier transport across the mirror layers is avoided resulting in a reduction of the series resistance. Impurity induced disordering of the quantum well with the diffusion of Si and Zn for the n

and p contacts, respectively, is applied. The top mirror is obtained by e-beam evaporation of Si/SiO₂. The top mirror evaporation is done after the structure is tested for electroluminescence such that adjustments on the dielectric layers thicknesses can be done for a fine adjustment of the resonance of the cavity to the electroluminescence peak. We have found that it is extremely difficult to obtain reflectivities above 99% with this material due to probably interface scattering and stoichiometry control of the SiO₂ deposition. Devices with single quantum well active region have emitted strongly at around 0.98 μ m wavelength, however laser operation was not observed. We believe the mirror loss on the top mirror is too high to allow the single quantum well to provide enough gain for lasing. Nevertheless, since no emission is observed at wavelengths near the GaAs band gap is a good indication of an efficient carrier injection obtained by the lateral injection scheme. Fig.1 shows a picture of one of these devices along with the measured spectrum with the device cw biased at 2.5 mA. In order to overcome the unbalance of gain and loss in these previous structure new designs are being currently implemented. In these structures lasers with two, three and four strained quantum wells are properly positioned in the cavity to increase the available gain. Since the strain builds up as more well are added to the structure, the spacing between wells has to be increased to release this strain. This imposes a limitation on the number of wells that can be used for a full wavelength cavity length and an effective injection. These structures were successfully grown as characterized by reflectivity spectrum and room temperature photoluminescence measurements. We are currently working on the fabrication of these devices. New materials for the dielectric top mirror are to be used. The dielectric pair, MgF/SbS, is showing to provide a higher reflectivity than Si/SiO₂ and may improve the device performance.

A second approach for surface emitting laser employs the use of etched 45° mirror on a conventional edge emitter device. The device is grown on top of a Bragg reflector. The light travels in a waveguide along the direction of quantum well and at the mirrors it undergoes a total internal reflection that sends it towards the back of the substrate. In this direction, the beam is partially reflected by the Bragg mirrors for the laser feedback and decoupling from the device as laser light output. In this approach the gain path is much longer and the mirror reflectivity requirements are relaxed. Also, since the spacing between modes in this longer Fabry-Perot cavity is much smaller than in the vertical cavity structure, the spontaneous emission linewidth can incorporate several resonance modes and the task of matching the well emission to one of these modes is much easier.

In order to obtain the lateral optical and electrical confinement for a narrow structure with low threshold we have chosen the temperature engineered growth developed in our group for low threshold AlGaAs/GaAs lasers (2). In this

technique, the growth is done on pre-patterned mesas on the substrates. Using the dependence of the growth rate of AlGaAs material on growth facets and growth temperature one can control the growth profile to obtain a buried structure after a single step MOCVD growth. We have obtained TEG lasers with single strained In_{0.2}Ga_{0.8}As. Devices with 1 mm stripes with pulsed operation threshold as low as 3 mA with 88% external at 1.0 mm were obtained (3). These results are among the best results for strained quantum well lasers and shows that the variations of temperature during the growth does not compromise the quality of the strained active region material. Also, no anomalous behavior of the InGaAs quantum wells on the side walls caused by a possible excessive strain was observed. In fact, optical and current confinement was found to be more effective than for AlGaAs devices probably due to a higher In composition on the mesa top.

After the successful results with the lasers grown on structured substrate, the application of a similar technique for surface emitting lasers was initiated. Two different approaches were taken for the growth of these devices. In the first case, two growth steps are employed. In the first step, the Bragg reflector is grown with a 5 mm GaAs cap for further processing. The reflectivity of the sample is checked and mesas for growth of a TEG laser are patterned. The second growth step consists of the TEG single strained quantum well laser growth. In the second case, the mesas are patterned on the substrate, the mirror layers and the TEG laser are grown in a single step growth. The entire structure with lateral optical and electrical confinement is thus obtained. These structures required an optimization of the growth conditions. The extreme difficulty of growing AlAs on the mesa sides due to the high reactivity and small mobility of this surface species made this growth of the Bragg structure on the mesa difficult.

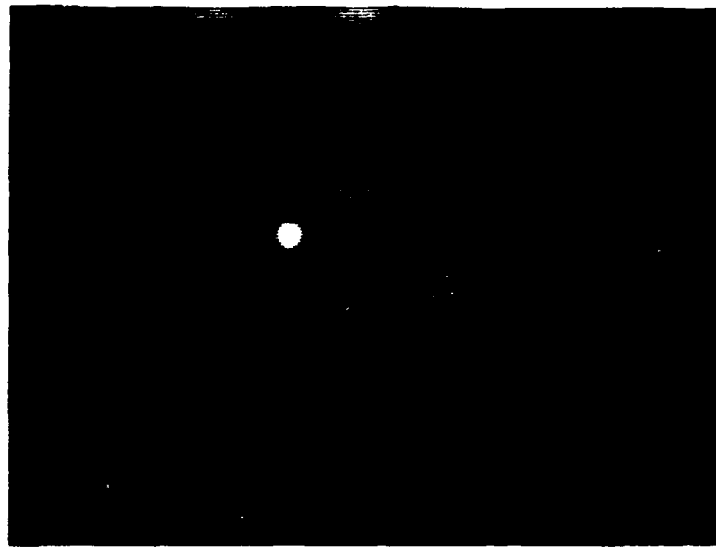
Fig. 2a shows a SEM cross section picture of a device of the second type after the contacting Zn diffusion was done. One can clearly see the different growth behavior on the mesa top and mesa side wall resulting in a sharp bending of the layers that should provide optical and electrical confinement similar to that observed in the conventional TEG lasers. These samples were fabricated into edge emitters as a test for the structure. The edge emitter devices with active region widths of 7.6, 5.1, and 3.4 mm resulted in pulsed threshold currents as low as 15, 12, and 15 mA with an average of 2.9 mA/mm with lasers emitting at 0.98 mm with approximately 84% external quantum efficiency. Some confinement problem may be present since the narrowest device has a threshold current of 4.4 mA/mm - not scaling linearly with the active region layer width. The I-V characteristics are very encouraging with reverse and forward bias resistance of 3.6×10^5 and 7 ohms, respectively. This indicates that the Bragg mirror is not increasing the series resistance nor it is creating any leakage mechanism. Fig. 2b shows the L-I and I-V plots for one laser with 5.0 mm active

region driven cw. The threshold is increased by 2.0 mA probably due to heating since no heatsink was used. We are also currently in a final stage of the processing of these structures for surface emitting lasers. In this first attempt, we have chosen devices with wide active regions (around 8 μm) to minimize any coupling loss of the optical beam as it leaves and reenters the wave-guide region. Narrower structures, as well as active regions with more than one strained quantum well, should also be studied in order to achieve the ultimate low current threshold.

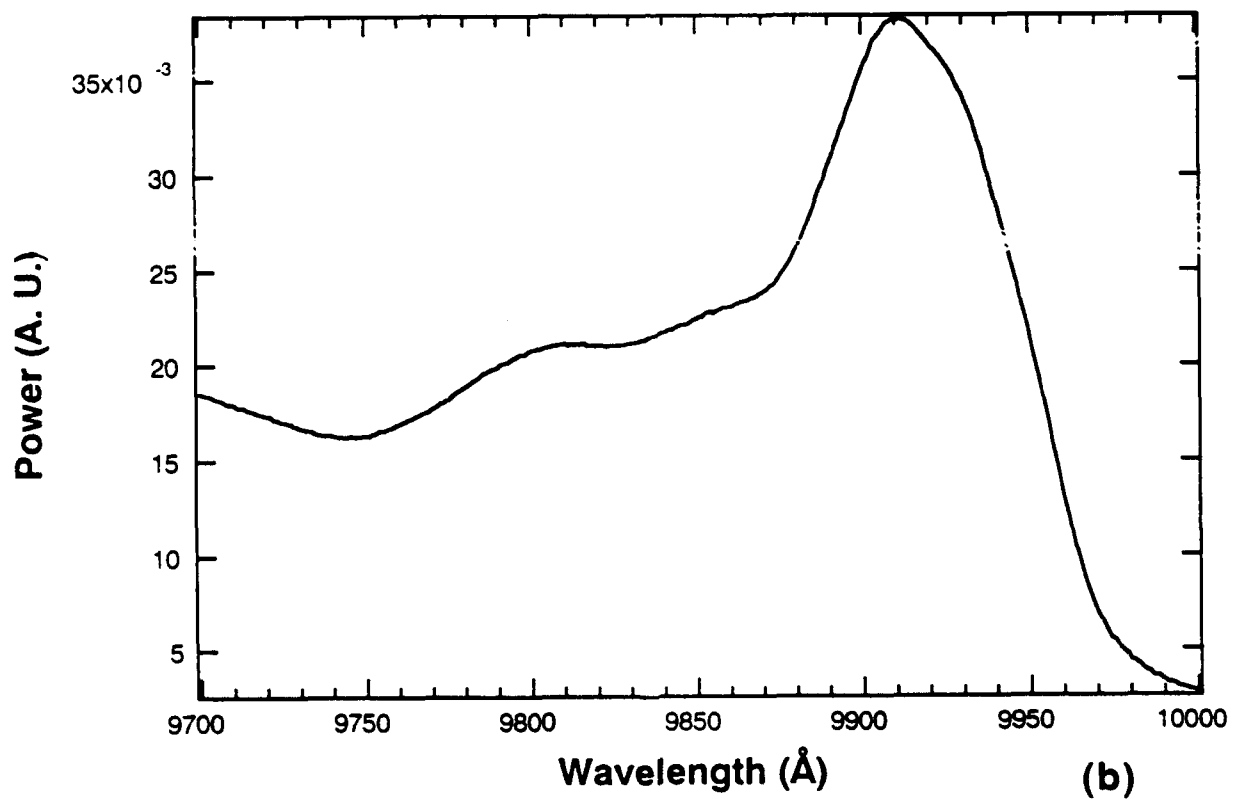
In conclusion, structures for the fabrication of vertical cavity surface emitting lasers with multiple strained quantum wells were successfully grown by MOCVD employing laser reflectometry technique. Single quantum well structures employing Si/SiO₂ mirrors was found to provide insufficient gain to overcome the mirror losses. Another approach for surface emitting laser utilizing 45° mirrors on lasers grown on structured substrates with a bottom AlAs/GaAs Bragg mirror was obtained. The results for edge emitter structures are very encouraging and surface emitting lasers utilizing these structures are in a final stage of processing in collaboration with TRW.

REFERENCES

- (1) N. C Frateschi, S. G . Hummel, P. D. Dapkus, Electron. Lett., vol. 27, p. 155, Jan. 1991.
- (2) K. M. Dzurko, E. P. Menu, C. A. Beyler, J. S. Osinski, and P. D. Dapkus, Appl. Phys. Lett., vol.54, p. 105, 1989.
- (3) N. C. Frateschi, J. S. Osinski, C. A. Beyler, and P. D. Dapkus, Photon. Technol. Lett., vol.4, p. 209, Mar 1992.

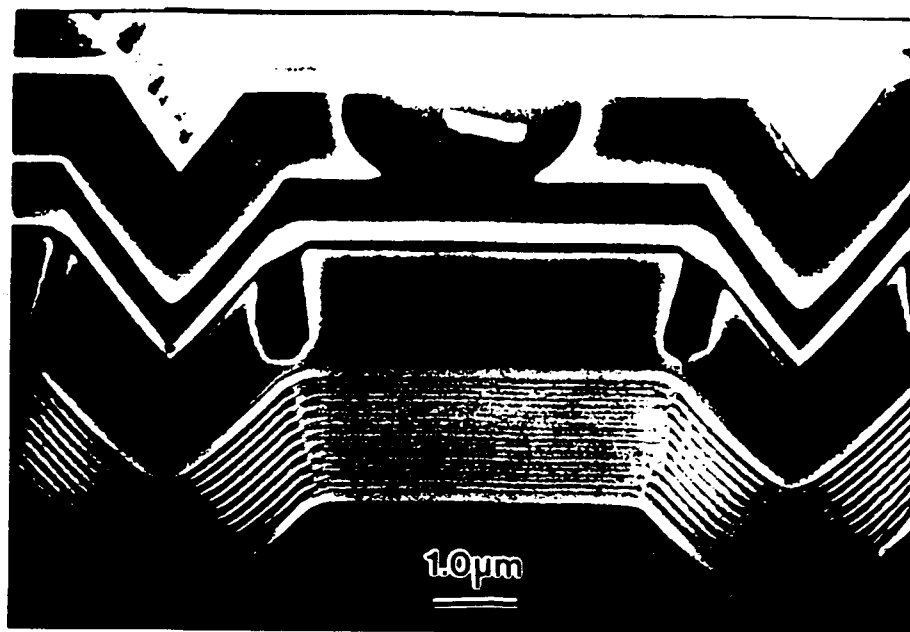


(a)

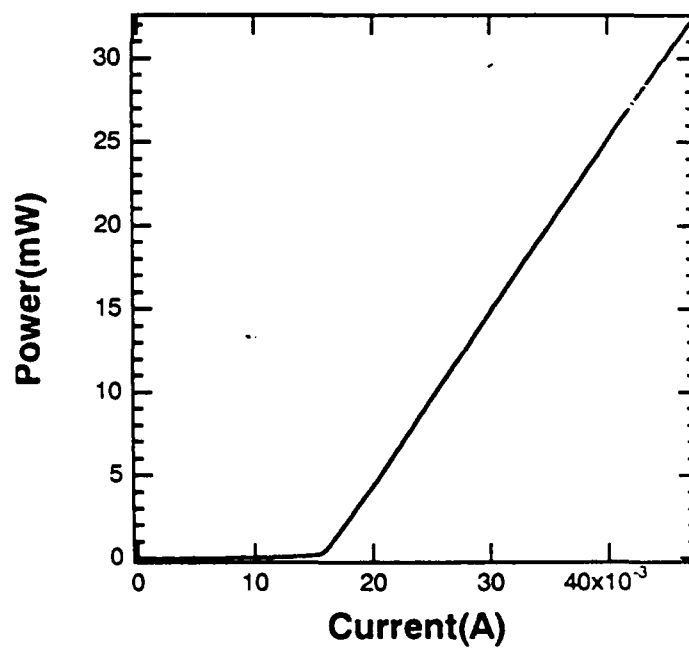
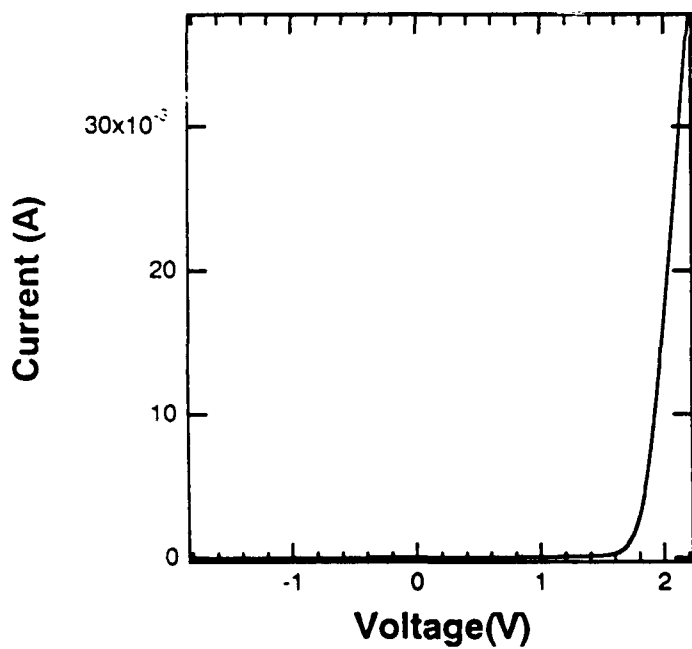


(b)

Fig.1 a) Lateral Injection structure for VCSEL. driven at 0.5 mA.
b) Measured spectra for this device driven cw at 2.5 mA.



(a)



(b)

Fig.2 a) SEM cross section of a laser structure with integrated Bragg reflector. b) $I \times V$ and $L \times I$ for this structure processed as an edge emitting laser.

Optical Interconnects And Optical Neurons Using Charge Transport Optical Nonlinearities

W. H. Steier

Real time holographic interconnection elements are key to the realization of optical neural networks. The advantages of arrays of mutually incoherent lasers for the writing and reading of these interconnects in a generalized neural network architecture have been discussed by Tanguay, Jenkins, and Madhukar in other sections of this report and our earlier reports. In these and other proposed architectures the preferred sources are semiconductor lasers which currently are well developed only in the infrared (0.9 to 1.5 μ m). In addition, the learning or iteration times for these systems should be on the order of one millisecond or less and the required optical energy should be as small as possible to avoid thermal problems. All of these requirements point to the use of photorefractive semiconductors as the real time holographic media. The semiconductors (CdTe, GaAs, InP) are sensitive in the IR, have photorefractive response times of tens of microseconds, and one of them (CdTe) has the highest measured photorefractive sensitivity(index change per absorbed photon) of any material. Based on this we have been making a systematic study of the semiconductors, measuring their photorefractive properties, calculating the possible interconnect capacities, and collaborating with industry(Brimrose Corp. and Hughes Research Laboratories) to help make available large high quality crystals.

The Capacity of Photorefractive Semiconductor Interconnects.

While the semiconductors have the advantages listed above and may be the only reasonable fast, infrared, real time holographic material available, they all share the major limitation that the maximum change in the index of refraction is limited to 10^{-4} to 10^{-5} . This is in contrast to the much slower and less sensitive oxides where index changes of 10^{-2} to 10^{-3} are possible. Therefore the systems design must be such that it makes optimum use of the limited Δn and accommodates the required E fields (possibly DC or AC) required to give the maximum Δn .

We have completed a preliminary study of the possible capacity of a semiconductor interconnect based on our measurements of the photorefractive properties of the semiconductors. For limited Δn it is generally advantageous to use the assigned volume hologram approach rather than the shared volume approach. For interconnecting N inputs to

N outputs, the hologram is divided into N sub-holograms each containing N gratings. Assuming the available Δn is shared equally by each grating, the strength of each grating is therefore $\Delta n/N$. The assigned volume also eliminates coherent interference effects on fan-in since the various outputs are angularly separated. To increase the Δn , one must apply either DC or alternating electric fields to the material with some sacrifice in response time.

In this analysis the number of interconnects is limited by the scattering of the material and the limited Δn . The output from any one grating must be several times the scattered intensity in that same direction. Based on this the maximum number of interconnects for the assigned volume hologram is:

$$N = 1.6\pi^3 L^3 (\Delta n)^2 / \lambda^4 \alpha_s$$

where

L = interaction length

λ = the wavelength of operation

α_s = the scattering coefficient of the material.

For $L = 1\text{cm}$, $\lambda = 1\text{mm}$, $\Delta n = 2.4 \times 10^{-5}$, $\alpha_s = 10^{-2}\text{cm}^{-1}$, the maximum number of interconnects is

$$N_{\text{max}} = 400.$$

This can be compared to a similar calculation for the shared volume hologram which predicts a maximum capacity of 125 interconnects.

There are several other effects that must be considered to complete this analysis. We have observed electric field shielding effects for both DC and alternating fields and this will effect the index change and possibility cause crosstalk between sub-holograms.

There are also questions concerning the sensitivity of the writing to the angle between the writing k vectors and the direction of the applied electric field. These issues and an experiment to demonstrate the capacity of semiconductor interconnects are being considered.

Development of CdTe, Cd_(1-x)Zn_xTe and ZnTe Photorefractive Semiconductors

In cooperation with Hughes Research Laboratories and Brimrose Corporation we have proceeded with a basic study of CdTe, ZnTe, and the mixed crystals Cd_(1-x)Zn_xTe. CdTe has a band gap near 0.9 μm and has possible photorefractivity from 0.9 μm out to 1.8 μm . ZnTe has a band gap near 0.6 μm and therefore has potential photorefractivity from the visible into the infrared. By varying the Cd, Zn mixture, a crystal can be grown

with a band gap anywhere over the 0.9 to 0.6 μm range and potential photorefractivity or other band edge effects over a wide range of wavelengths.

The CdTe is vanadium doped for charge compensation to provide high resistivity material ($10^{10}\Omega\text{-cm}$) and to be a possible source of deep level traps for photorefractivity. Typical starting concentrations of V are 10^{19}cm^{-3} . Two wave mixing gain measurements showed an effective trap density of $2 \times 10^{15}\text{cm}^{-3}$ and $\xi r_{41} = 4.4\text{pm/V}$, where r_{41} is the electrooptic coefficient and ξ is the electron-hole competition factor. Two beam coupling was measured at 1.06 μm , 1.3 μm , and 1.52 μm . Typical maximum gains of 0.6cm^{-1} were observed near 1 μm grating spacing and are shown in Figure 1. The equivalent dark irradiance was $88\mu\text{W/cm}^2$ and consequently a $\mu\tau$ product in the 10^{-6} - 10^{-5} range. The measured index change per absorbed energy per volume was $0.51\text{cm}^3/\text{J}$; at least an order of magnitude larger than any other material. At an intensity of 10W/cm^2 the response time was a few microseconds.

We have measured the photorefractivity of vanadium-doped ZnTe in the 630 to 1300 nm wavelength range. There is an ongoing need for improved photorefractive materials at diode laser wavelengths in the 800-900 nm region for several applications. Cubic and ferroelectric oxides lack the required fast and efficient response at these wavelengths while the semiconductors such as CdTe and GaAs have their operating wavelengths limited to greater than 900 nm. We have now shown that ZnTe is a very efficient photorefractive material to fill this need. Two wave mixing gain measurements at 630 nm show a maximum gain of 0.45cm^{-1} at a fringe spacing of 2 μm . From these measurements a trap density of $1.4 \times 10^{14}\text{cm}^{-3}$ and $\xi r_{41} = 4.17\text{pm/V}$ were derived. This is a relatively low trap density in comparison to other semiconductors ($5 \times 10^{15}\text{cm}^{-3}$) and suggests that by altering the growth slightly, larger trap densities and gains up to 1.2cm^{-1} may be possible. The fastest grating formation time we observed was 14.7 μs used at 4.7W/cm^2 which is comparable to GaAs and confirms ZnTe as a fast red-NIR photorefractive material.

We have undertaken the study of photorefractivity in II-VI alloys of CdTe and observed beam coupling gain at 1.318 μm in $\text{Cd}_{0.94}\text{Zn}_{0.06}\text{Te}:\text{V}$ samples. To the best of our knowledge this is the first observation in ternary II-VI compounds. The bulk alloying capability can lead to the development of materials whose band gap and sensitivity range can overlap the wavelength of application. The measured resistivity was $10^7\Omega\text{-cm}$ and

the observed gain was 0.22 cm^{-1} at $\lambda = 1.34 \text{ }\mu\text{m}$. The absorption at $1.3 \text{ }\mu\text{m}$ was less than 0.1 cm^{-1} . The derived trap density was $2 \times 10^{15} \text{ cm}^{-3}$ and $\xi_{r41} = 3 \text{ pm/V}$.

Enhancement of the Photorefractive Gain at 1.3 - 1.5 μm in CdTe Using Alternating Electric Fields

The magnitude of the photorefractive index change in semiconductors is usually small and gain enhancement techniques such as dc fields or ac fields are required. We used the applied alternating field (ac) method with square and sinusoidal waveforms and report gain coefficients in excess of 10 cm^{-1} at $1.3 \text{ }\mu\text{m}$ which significantly exceed the absorption coefficient of 2 cm^{-1} in our sample. This dramatic increase in the gain that can be achieved using alternating electric fields is shown in Figure 2. Our measurements show that the parameters of the ac waveform such as frequency and rise time play a significant role and can impose severe limits on the achievable gain. The limits are discussed in detail in the relevant publication.

Beam Coupling Gain at 1.3 μm and 1.5 μm

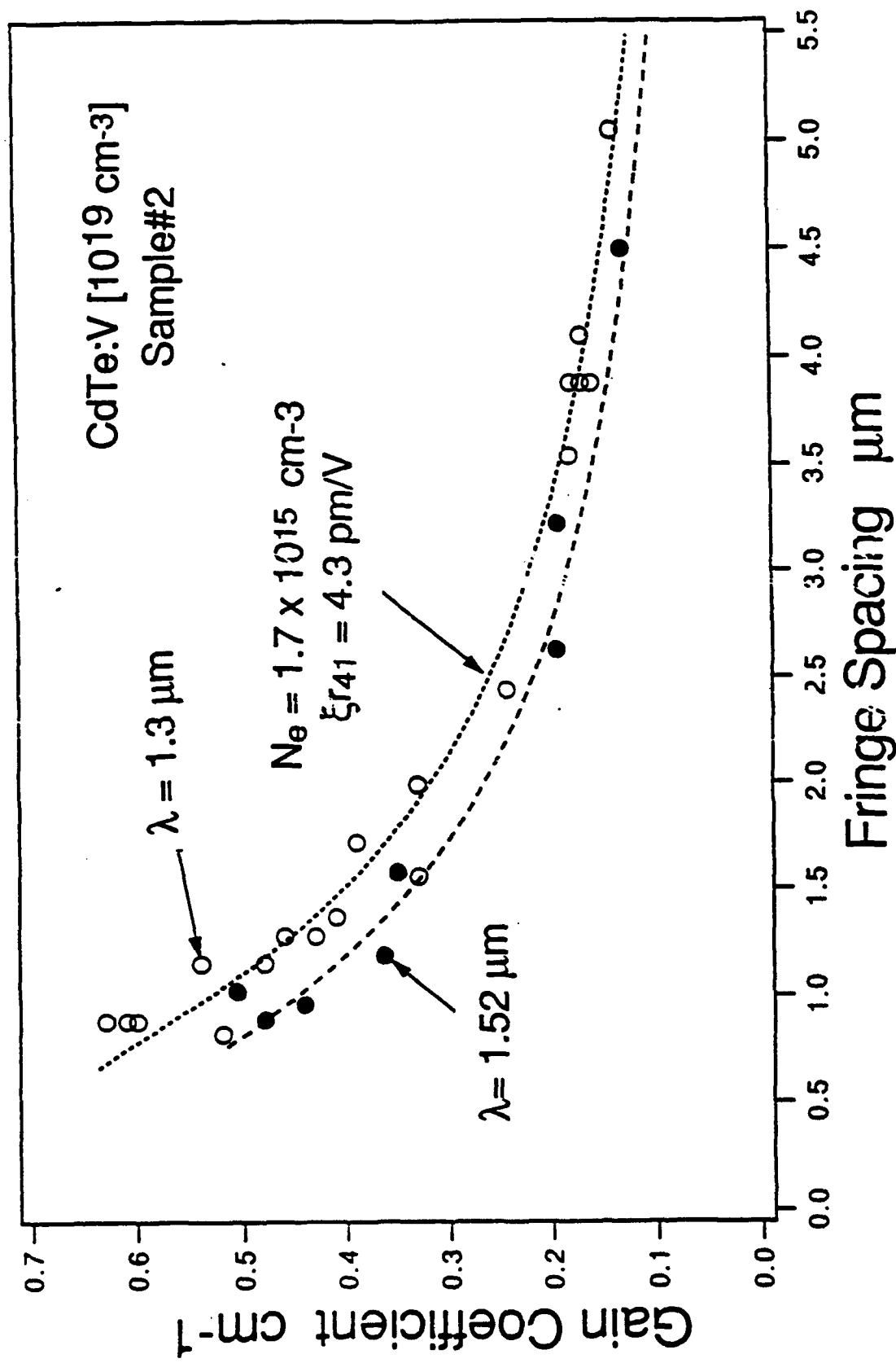
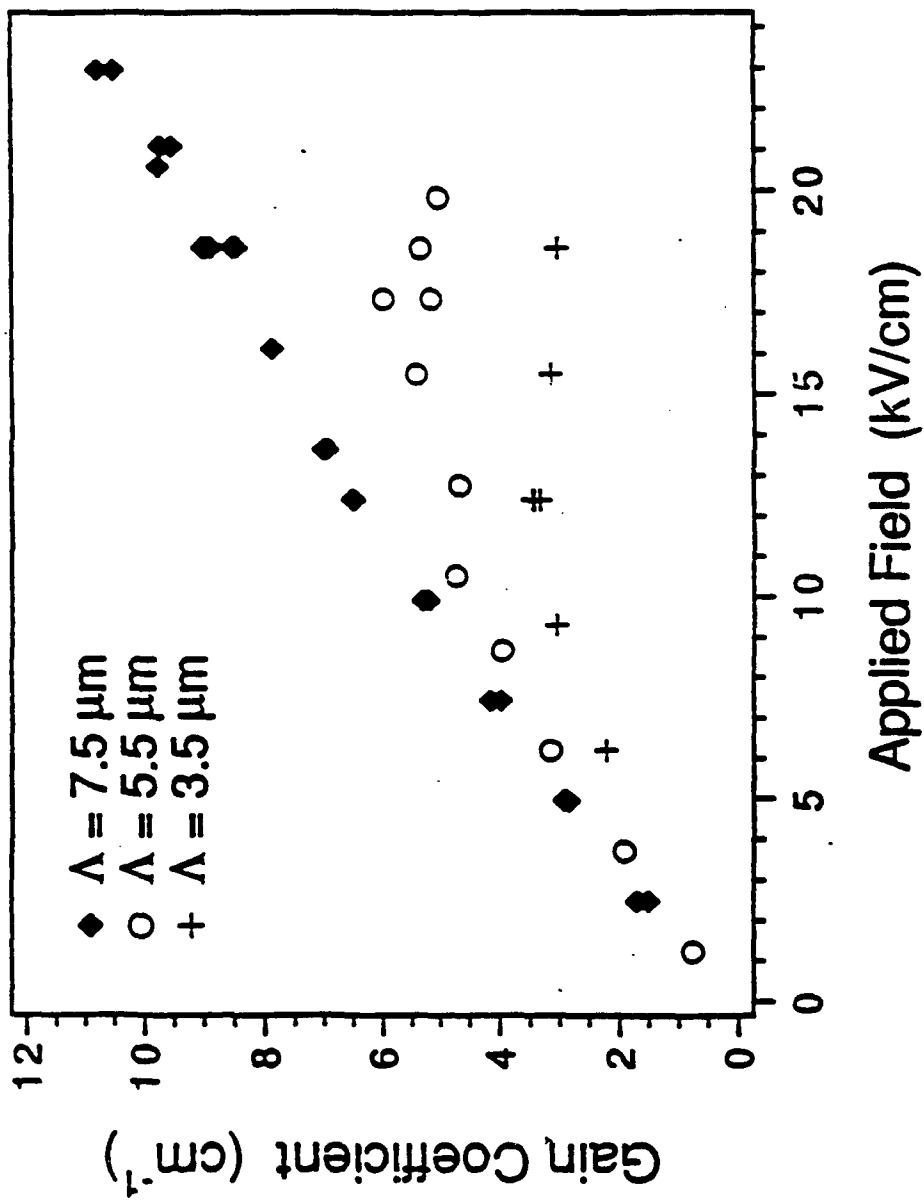


Fig. 1
Beam coupling gain of CdTe:V

Fig. 2
 Alternating electric field enhanced gain in CdTe: V



Optical Interconnections Using Wave Mixing at the Bandedge in III-V Semiconductor Depletion Regions

E. Garmire

This project explores nonlinear optical interconnects using wave mixing. Large nonlinearities are required to achieve efficient beam deflection and suggests that quantum wells should be used for this application.

We have found that optical nonlinearities in QW are not yet large enough to make good optical interconnects. We are thus continuing to explore the nonlinearities of multiple quantum wells (MQW) placed in n-i-p-i structures in order to improve their performance. Research is underway in both psec and cw measurements, in order to determine the bottleneck to achieving larger nonlinearities. In time-delay pump-probe experiments, the rise-time of the signal gives the tunneling time and the fall time shows the effect of enhanced diffusion out of the focal spot. Our original measurements have been made using p-i-n structures and applied voltages to ensure our understanding of the microscopic processes. Of interest is the fact that our tunneling times are much shorter than in GaAs/AlGaAs quantum wells.

In order to further understand the limits to achieving higher nonlinearities, we are supporting the psec measurements with cw measurements of nonlinear response, both in n-i-p-i structures and in p-i-n structures with a field applied. The latter structures allow us to know exactly what the internal fields are and to better analyze the results. We have found that with increased pumping, a n-i-p-i MQW transmission increases and then saturates at relatively low power levels (Figure 1). However, when the pumping level is increased, the sample again starts to increase in transmission change. We originally attributed this to an onset of band-filling. Now, however, further experiments measuring the spectral response indicate that all these effects may still be due to changing internal fields. Further investigation is required to understand this. We are carrying out experiments to measure the wavelength dependence of this nonlinearity to determine the mechanism.

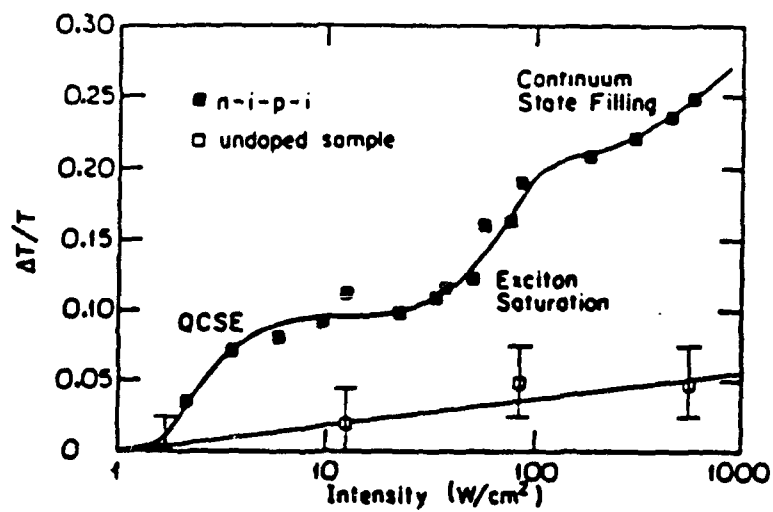


FIG. 1 Single pass transmission of a highly intensity beam focused onto a multiple quantum well hetero $n-i-p-i$ sample and a second undoped sample with identical quantum wells. The origins of the increasing transmission for the $n-i-p-i$ are indicated for corresponding regions of intensity.

Photorefractive Optical Interconnections

J. Feinberg

We have completed our investigation into the use of a photorefractive crystal as an optical switchboard for interconnecting many optical channels. We constructed a device that will connect any of N input channels to any of M output channels. The device uses a photorefractive crystal of BaTiO_3 as a mutually-pumped phase conjugator in a "bird-wing" geometry. To connect two channels one simply directs light into each of the channels and the conjugator automatically connects them. The two injected light beams should have the same nominal wavelength, but it is preferable that the light beams not be coherent with each other.

In our previous design, we used a bundle of fibers to carry the separate signals to and from the phase conjugator. One problem with this old design is that some input and output channels overlapped better than others in the crystal, resulting in large variations in the throughput for different channels. In our new design, we used a tapered fiber to combine and scramble all of the incoming signals before they reach the phase conjugator. The advantage of this new design is that the spatial overlap of all of the channels is now uniform, so that the throughput of the device is the same for any channel. We use the unscrambling capability of the phase conjugator to direct the signal to the proper output channel.

Because the tapered fiber depolarized the incident light beams, we had to construct a mutually-pumped phase conjugator that would work equally well for an arbitrary light polarization. A bird-wing phase conjugator made from a BaTiO_3 crystal only works for light that is polarized to be an extraordinary ray. Therefore, we used a polarizing beam splitter to separate the s and p polarizations from each tapered fiber, and a half-wave plate to rotate the s polarization 90° before it entered the BaTiO_3 crystal. We adjusted the optical path-length difference between the s and p polarized beams to be well within the coherence length of the laser. Two small prisms attached to the crystal made the input beam angles ideal for the crystal to operate as a "bird-wing" mutually-pumped phase conjugator.

We measured the transmission efficiency from each of 4 channels A_i to each of 4 channels B_j and vice versa; for all 32 measurements the transmissivity was always $(12 \pm 1)\%$. For these measurements we first adjusted the input powers so that, at the crystal, $P_{A_i} = P_{B_j} = 2 \text{ mW}$ for

each A and B channel. We selected individual channels by translating the stages holding the fiber arrays, but we kept the alignment of the rest of the optical system fixed. The fact that the transmissivities were so similar for connecting any of the A channels to any of the B channels, and vice versa, implies that the light from the A taper was always overlapping well in the crystal with the light from the B taper. The problem of non-overlapping channels was solved.

The overall system transmissivities, including losses from coupling into and out of each of the 8 different input fibers, ranged from 1.5% to 9.8%, depending on the particular channels selected, and so were smaller than the transmissivities of the conjugator alone by a factor ranging from 1.3 - 5. The reduced transmissivity was due, in part to the fact that the beam headed from the crystal into a fiber taper was an imperfect phase-conjugate replica of the beam coming out of the taper, caused partly by the imperfect collection of each fiber's light by the small-aperture objectives, and especially by the easily observable scattering at the cleaved end of the fiber tapers. The resulting loss of information caused imperfect phase-conjugate reconstruction, which then caused inaccurate coupling back into the tapered fiber. Indeed, microscopic inspection revealed that the A taper had a worse cleave than the B taper, and we could see that the crystal directed more light in the wrong direction at the A taper than at the B taper. To improve the overall transmissivities, we need well-cleaved or even polished fiber tapers and objective lenses having a large numerical aperture. The typical measured interchannel crosstalk was $\sim 15\%$ (defined here as the signal power in an incorrect channel divided by the signal power in the correct channel). Again, if all of the light coming out from the taper had been collected and sent into the crystal, the interchannel crosstalk should have been zero.

We found it essential to use both polarization components to make a connection through the crystal. Using only one polarization component decreased the coupling efficiency of the conjugate beam into the fiber taper by a factor of 30%, and it also doubled the interchannel cross-talk. Additionally, the two polarization components must be coherent with each other both at the crystal and at the fiber. If not, they will erase each other's fanning gratings in the crystal. Even worse, the two phase-conjugate beams for the two polarizations will not recombine coherently in the fiber to reconstruct the correct phase front, and so will increase the interchannel crosstalk.

The transmission bandwidth of this device is limited by the modal dispersion of the fiber taper, the Bragg-matching bandwidth of the photorefractive grating in the crystal, and the group velocity dispersion of the crystal. When using rapidly modulated light to establish the grating, the modal dispersion of the fiber taper will decrease the spatial coherence of the light coming out of the fiber taper, and this will decrease the interconnection efficiency. We estimate that a one-meter long multimode fiber taper having a numerical aperture of 0.22 limits the maximum data rate to 200 Gb/sec. For a sufficiently short fiber taper the data rate is then limited by the finite Bragg-matching bandwidth of the photorefractive grating, which we estimate to be 1 THz, corresponding to a maximum data rate of 1000 Gb/sec. Using the known group-velocity dispersion in BaTiO₃ of 7.266 (ps²/m) for e rays at 515 nm, we calculate that for a 5 mm long crystal the maximum data rate is 3000 Gb/sec. Experimentally we successfully operated the bird-wing conjugator without the fiber taper using sub-picosecond pulses from a sync-pumped dye laser, which corresponds to a data rate of ~1000 Gb/sec. We also calculate that the coupling efficiency of the signal back into the tapered fiber will decrease and interchannel crosstalk will markedly increase if the wavelength difference of the A and B channel lasers exceeds 0.5 nm.

In summary, we have demonstrated a fiberoptic interconnection device based on a mutually-pumped phase conjugator. The conjugator automatically routes light from selected information-sending channels to selected information-receiving channels, and vice versa. The phase-conjugating property of the device eliminates the need for critical alignment. In principle, we can make the device very compact, and so interconnect a large number of optical fiber channels.

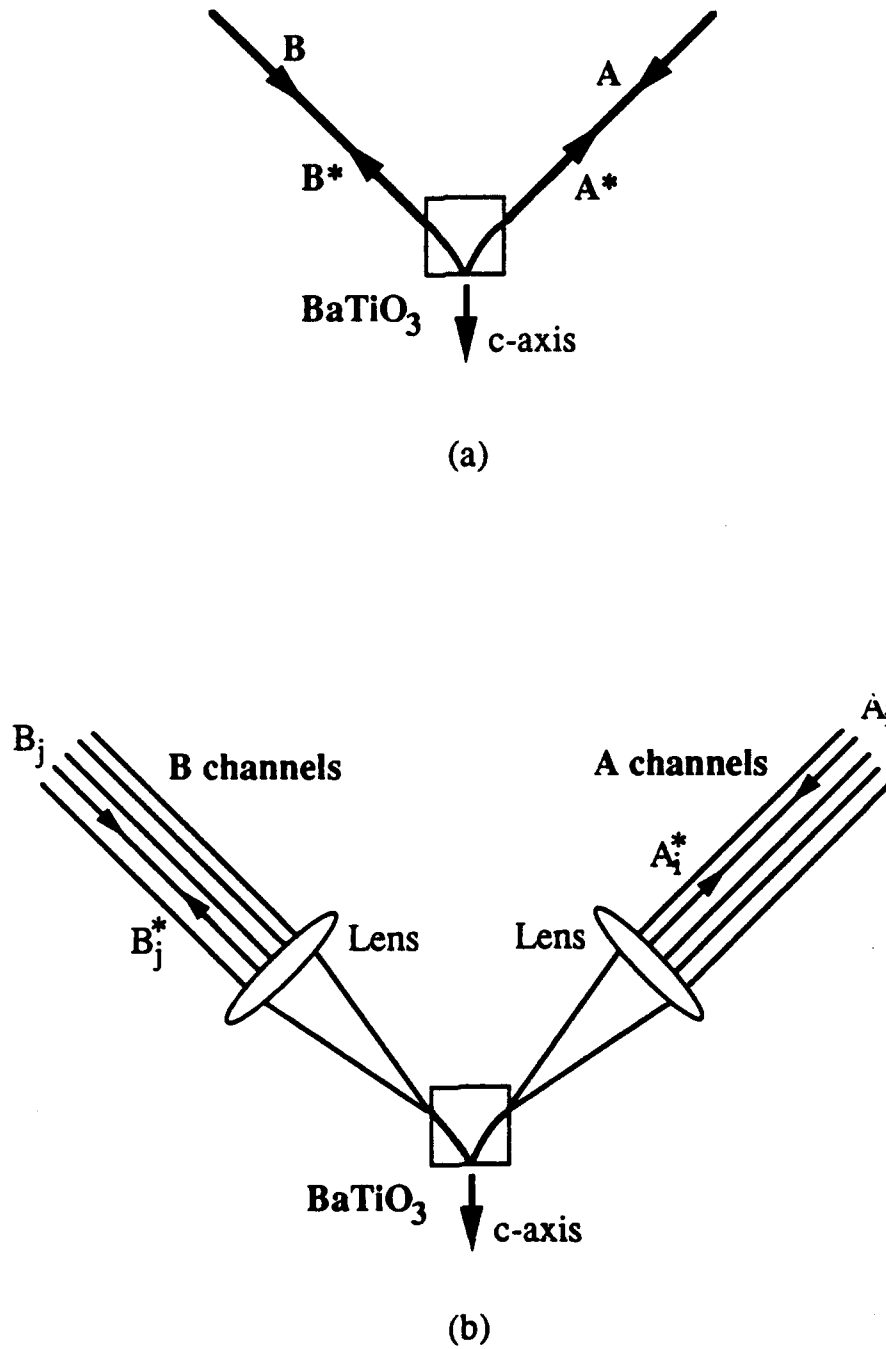


Figure 1
(a) Simple bird-wing conjugator. Beams A and B are the same nominal wavelength but are mutually incoherent. (b) A simple interconnection device using the bird-wing conjugator. The lens at each side of the crystal focuses the parallel beams of all the channels to a single spot in the crystal.

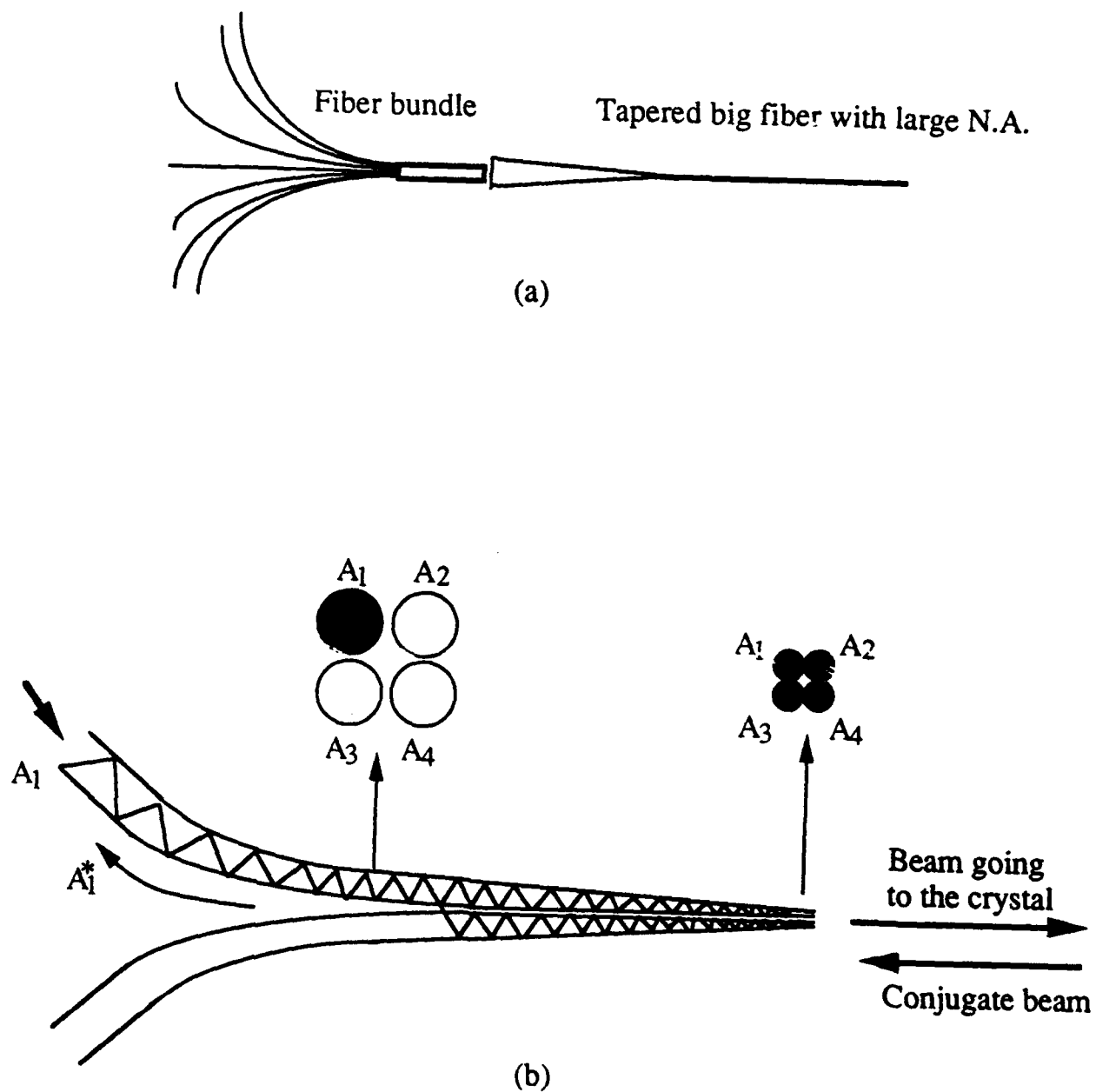


Figure 2
 (a) A single, large, tapered fiber is used to convert each channel's position information in the fiber bundle into a unique mode pattern. (b) A tapered fiber bundle accomplishes the same task.

PUBLICATIONS AND PRESENTATIONS

1. "Volume Holographic Techniques For Highly Multiplexed Interconnection Applications," P. Asthana, Ph.D. Dissertation, University of Southern California, Los Angeles, California, (1990).
2. "Electrooptic Materials Requirements for Optical Information Processing and Computing," P. Asthana, E. J. Herbulock, Z. Karim, C. Kyriakakis, G. P. Nordin, and A. R. Tanguay, Jr., to appear in Materials Research Society Proceedings, Vol. 228 (1992), for the 1991 MRS Spring Meeting; (Invited Paper).
3. "High Contrast Ratio Asymmetric Fabry-Perot Reflection Spatial Light Modulator Based on GaAs/InGaAs Multiple Quantum Wells," K. Hu, L. Chen, A. Madhukar, P. Chen, K. C. Rajkumar, K. Kaviani, Z. Karim, C. Kyriakakis, and A. R. Tanguay, Jr., Appl. Phys. Lett., **59** (9), pp. 1108-1110 (1991).
5. "The Growth and Performance of Strained InGaAs/GaAs Multiple Quantum Well Based Asymmetric Fabry-Perot Reflection Modulators", K. Hu, L. Chen, R. Kapre, K. C. Rajkumar, A. Madhukar, Z. Karim, C. Kyriakakis, and A. R. Tanguay, Jr., Proc. of the IEEE-LEOS 1991 Summer Topical Meeting, (July 29-31, Newport Beach, CA), p. 18.
6. "Photonic Implementations of Neural Networks", B. K. Jenkins and A. R. Tanguay, Jr., Chapter 9 in *Neural Networks for Signal Processing*, B. Kosko, Ed., Prentice Hall, Englewood Cliffs, New Jersey, (1992).
7. "A Single-Step Copying Process for Multiplexed Volume Holograms", S. Piazzolla, B. K. Jenkins, and A. R. Tanguay, Jr., accepted for publication in Optics Letters, (in press, 1992).
8. "Combined local and carrier transport optical nonlinearities in a hetero n-i-p-i structure", A. Kost, M. Jupina, E. Garmire, and T. C. Hasenberg, Appl. Phys. Lett. **58**, 1018-1020 (1991)
9. "Effect of front-facet reflections on the reflectivity of Bragg reflectors", B. G. Kim and E. Garmire, Opt. Lett. **16**, 1065-1067, (1991)

10. "Comparison between the matrix method and the coupled wave method in analyzing Bragg Reflector structures", B. G. Kim and E. Garmire, *JOSA A*, 9, 132-136, January, 1992.
11. "Electro-absorption and electro-refraction in InAs/GaAs short period superlattices", M. Jupina, E. Garmire, A. Kost and T. C. Hasenberg) *Applied Physics Letters*, February, 1992.
12. "Two beam coupling with high gain, operating near the band-edge of semiconductors", E. Garmire invited talk at the 1991 Gordon Conference on Nonlinear Optics and Lasers.
13. "Carrier transport in hetero-n-i-p-i's modeled as a photorefractive medium with deep traps", D. Magharefteh and E. Garmire to be presented at the MRS Mtg., San Francisco, May, 1992.
14. "Electro-absorption and electro-refraction in InAs/GaAs short period superlattices M. Jupina, S. Koehler, E. Garmire and A. Kost presented at the OSA Annual Meeting, November, 1991
15. "Electro-absorption and electro-refraction in InAs/GaAs strained layer MQW at wavelengths below the band-edge," S. D. Koehler, D. Yap and E. Garmire to be presented at CLEO.
16. "3-D Omega Networks for Optical Implementation," L. Cheng and A. A. Sawchuk, to appear in *Applied Optics*.
17. "Optically Powered 2x2 Optoelectronic Switch with Polarization Routing," M. Govindarajan, S. R. Forrest, L. Cheng and A. A. Sawchuk, *IEEE Photonics Technology Letters*, vol. 3, pp. 669-672, (1991).
18. "Holographic Implementation of 2-D Perfect Shuffles Based on a One-Copy Algorithm," J.-M. Wang, L. Cheng and A. A. Sawchuk, in *Photonic Switching 1991*, Technical Digest Series, Optical Society of America, Washington, DC 1991, pp. 180-183.
19. "Optical 2-D Perfect Shuffles Based on a One-Copy Algorithm," J.-M. Wang, L. Cheng and A. A. Sawchuk, to appear in *Applied Optics*.
20. "A One-Copy Algorithm for 2-D Shuffles for Optical Omega Networks," L. Cheng and A. A. Sawchuk, to appear in *Journal of Parallel and Distributed Computing*.

21. "Optically Powered Arrays for Optoelectronic Interconnection Networks", M. Govindarajan and S. R. Forrest, *Applied Optics*, vol. 30, 1335 (1991).
22. "Optically Powered, Integrated "Smart" Pixels for Optical Interconnection Networks", J. J. Brown, J. Gardner and S. R. Forrest, *IEEE Photonics Technol. Lett.*, vol. 3, 1136 (1991).
23. Topical Mtg. on Int. Photonic Res., J. J. Brown, J. Gardner and S. R. Forrest, *Tech. Dig.*, vol. 8, 11 (1991).
24. "Photorefractive Properties and Alternating Electric Field Gain Enhancement of Vanadium Doped Cadmium Telluride and Related Compounds," M. Ziari, W. H. Steier, M. B. Klein, and S. Trivedi, Paper TuA6, Conf. on Photorefractive Matr., Effects, and Devices, Beverly, Mass, July 29-31, 1991.
25. "Photorefractivity in Vanadium-doped ZnTe", M. Ziari, W. H. Steier, P. M. Ranon, S. Trivedi and M. B. Klein, accepted for publication in *Appl. Phys. Lett.*.
26. "Enhancement of the Photorefractive Gain at 1.5 - 1.3 μ m in CdTe Using Alternating Electric Fields", M. Ziari, W. H. Steier, P. M. Ranon, M. B. Klein and S. Trivedi, accepted for publication in *J. Opt. Soc.*
27. "Photorefractive Effect in ZnTe" M. Ziari, W. H. Steier, P. Ranon, M. B. Klein and S. Trivedi, to be presented at CLEO, Anaheim, Calif., May, 1992 .
28. "Optically Controlled Space Charge Fields Under the Electrode Region in Cadmium Telluride," M. Ziari and W. H. Steier, Paper D5.2, *Matr. Res. Soc. Mtg.*, San Francisco, May, 1992.
29. "Inverted Cavity GaAs / InGaAs Asymmetric Fabry-Perot Reflection Modulator", K. Hu, Li Chen, A. Madhukar, P. Chen, C. Kyriakakis, Z. Karim, and A. R. Tanguay, Jr., *Appl. Phys. Lett.* 59, 1664(1991).
30. "All Optical Photonic Switches Using Integrated *Inverted* Asymmetric Fabry-Perot Modulators and Heterojunction Phototransistors", K. Hu, Li Chen, K. Kaviani, P. Chen and A. Madhukar, *IEEE Photonics Tech. Lett.* (March 1992 issue, In Press).

31. "High Contrast Ratio Self Electro-optic Effect Devices Based on *Inverted* InGaAs / GaAs Asymmetric Fabry-Perot Modulators", Li Chen, K. Hu, R. M. Kapre and A. Madhukar, *Appl. Phys. Lett.* **60**, 422 (1992).
32. "High Contrast Ratio Optically Bistable Optoelectronic Switches Based on InGaAs / GaAs (001) Conventional and *Inverted* Asymmetric Fabry-Perot Modulators Grown via Molecular Beam Epitaxy", Li Chen, K. Hu, R. M. Kapre, W. Chen, P. Chen, and A. Madhukar, *Jour. Vac. Sci. Tech.* (March 1992 issue, In Press)
33. "High Contrast Optically Bistable Optoelectronic Switches Using Strained InGaAs / GaAs Material System", R. M. Kapre, Li Chen, K. Kaviani, K. Hu, P. Chen, and A. Madhukar, *MRS Proceedings*, Vol. 240, 1992 (In Press).
34. "Incoherent dynamic lenslet array processor for neural networks", D. Wiley, I. Glaser, B. K. Jenkins, and A. A. Sawchuk, *Technical Digest*, Optical Society of America Annual Meeting, paper FDD1, San Jose, CA, November 1991.
35. "Single-step copying technique for multiplexed volume holograms", S. Piazzolla, B. K. Jenkins, and A. R. Tanguay, Jr., *Technical Digest*, Optical Society of America Annual Meeting, paper FDD1, San Jose, CA, November 1991.
36. "In Situ Laser Reflectometry Applied to the Growth of $Al_xGa_{1-x}As$ Bragg Reflectors by Metalorganic Chemical Vapour Deposition", N. C. Frateschi, S. G. Hummel, P. D. Dapkus, *Electron. Lett.*, 155-156, **27**(2), 1991.
37. "Low-Threshold Single-Quantum-Well InGaAs/GaAs Lasers Grown by Metal-Organic Chemical Vapor Deposition on Structured Substrates", N. C. Frateschi, J. S. Osinski, C. A. Beyler, and P. D. Dapkus, *IEEE Photon. Technol. Lett.*, vol. 4(3), 209, March 1992.

PATENTS RESULTING FROM THIS GRANT

1. B. K. Jenkins and A. R. Tanguay, Jr., "Incoherent/coherent multiplexed holographic recording for photonic interconnections and holographic optical elements", USC-2254, allowed by USPTO, patent pending.

2. B. K. Jenkins and A. R. Tanguay, Jr., "Incoherent/coherent multiplexed holographic recording for photonic interconnections and holographic optical elements: spatial light modulator," USC-2254A, divisional, filing date April 6, 1990.
3. B. K. Jenkins and A. R. Tanguay, Jr., "Incoherent/coherent multiplexed holographic recording for photonic interconnections and holographic optical elements: source array," USC-2254B, divisional, filing date April 6, 1990.